frontiers | Frontiers in Energy Research

TYPE Review
PUBLISHED 31 May 2023
DOI 10.3389/fenrg.2023.1194674

Check for updates

OPEN ACCESS

EDITED BY
Xiahui Zhang,
Central South University, China

REVIEWED BY
Zhongxin Song,
Shenzhen University, China
Tauseef Anwar,
University of Lahore, Pakistan

*CORRESPONDENCE
Xuelian Li,
lixuelian@tyut.edu.cn
Lili Gao,
gaolili@tyut.edu.cn

†These authors have contributed equally to this work and share first authorship

RECEIVED 27 March 2023
ACCEPTED 16 May 2023
PUBLISHED 31 May 2023

CITATION
Guo W, Wang Y, Yi Q, Devid E, Li X, Lei P, Shan W, Qi K, Shi L and Gao L (2023), Research progress of aqueous Zn–CO_2 battery: design principle and development strategy of a multifunctional catalyst.
Front. Energy Res. 11:1194674.
doi: 10.3389/fenrg.2023.1194674

COPYRIGHT
© 2023 Guo, Wang, Yi, Devid, Li, Lei, Shan, Qi, Shi and Gao. This is an open-access article distributed under the terms of the Creative Commons Attribution License (CC BY). The use, distribution or reproduction in other forums is permitted, provided the original author(s) and the copyright owner(s) are credited and that the original publication in this journal is cited, in accordance with accepted academic practice. No use, distribution or reproduction is permitted which does not comply with these terms.

Research progress of aqueous Zn–CO_2 battery: design principle and development strategy of a multifunctional catalyst

Wenqi Guo[1,2†], Yukun Wang[1,2†], Qun Yi[1,3], Edwin Devid[4], Xuelian Li[1,2,5*], Puying Lei[1,2], Wenlan Shan[1,2], Kai Qi[1,2], Lijuan Shi[1,3] and Lili Gao[1,2*]

[1]College of Environmental Science and Engineering, Taiyuan University of Technology, Taiyuan, Shanxi, China, [2]Shanxi Key Laboratory of Compound Air Pollutions Identification and Control, Taiyuan University of Technology, Taiyuan, China, [3]School of Chemical Engineering and Pharmacy, Wuhan Institute of Technology, Wuhan, Hubei, China, [4]Plasma Solar Fuels Devices, Dutch Institute for Fundamental Energy Research (DIFFER), Nieuwegein, Netherlands, [5]Shanxi Zhongke Huaneng Technology Co.,Ltd., Taiyuan, Shanxi, China

Aqueous Zn–CO_2 battery possesses a large theoretical capacity of 820 mAh g^{-1} (5855 mAh cm^{-3}) and high safety, showing a unique position in carbon neutrality and/or reduction and energy conversion and storage, which has developed rapidly in recent years. However, obstacles such as low value-added products, low current density, high overvoltage, and finite cycles impede its practical application. Cathode catalysts, as a key component, have a significant influence on gas cell performance. Despite many updated papers on cathode materials for aqueous Zn–CO_2 batteries, a systematic summary has rarely been reported, and even less is mentioned about the design principle and development strategy for efficient catalysts. Relying on the structure and mechanism of the Zn–CO_2 battery, this review discusses the research progress and existing challenges, and, more importantly, the design strategies and preparation methods of the efficient cathode are proposed, centering on material structure, charge distribution, and coordination environment. Finally, in this review, the opportunities for the development of a high-performance Zn–CO_2 battery are highlighted, which enables enlightening the future exploration of next-generation energy storage systems.

KEYWORDS

Zn–CO_2 batteries, multifunctional catalysts, reaction mechanism, catalyst design strategies, single-atom catalysts

1 Introduction

Excessive carbon dioxide (CO_2) emissions caused by consumption of fossil fuels further aggravate the global energy crisis and the greenhouse effect (Chang et al., 2017; Asadi et al., 2018; Zhou et al., 2020). In recent years, the carbon capture, utilization, and storage (CCUS) (Chen et al., 2022c; de Oliveira Maciel et al., 2022; Jiang et al., 2022; Pfeiffer et al., 2022) technology has become a hot topic of research. Among them, metal–CO_2 batteries adopt CO_2 catalytic conversion and an energy storage solution where chemical energy is converted into green renewable electricity while reducing CO_2 emissions (Chu et al., 2016; Ahmadiparidari et al., 2019; Eskezia Ayalew, 2021). Compared with traditional ion

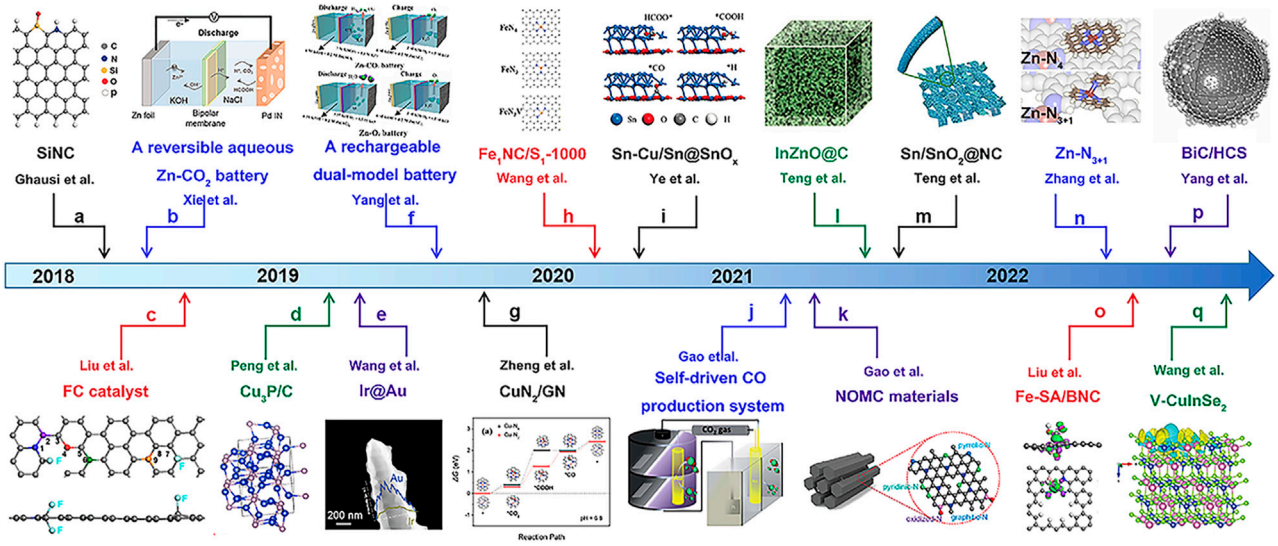

FIGURE 1
Timeline about the important developments of aqueous Zn–CO_2 battery systems and cathode catalysts. **(A)** F-doped carbon (FC). Reproduced with permission (Xie et al., 2018b). Copyright 2018, Wiley. **(B)** Porous silicon–nitrogen-co-doped carbon (SiNC). Reproduced with permission (Ghausi et al., 2018). Copyright 2018, Wiley. **(C)** Reversible aqueous Zn–CO_2 battery. Reproduced with permission (Xie et al., 2018a). Copyright 2018, Wiley. **(D)** Dendritic 3D Ir@Au. Reproduced with permission (Wang et al., 2019). Copyright 2019, Wiley. **(E)** Cu_3P/C nanocomposites. Reproduced with permission (Peng et al., 2019). Copyright 2019, American Scientific Publishers. **(F)** Rechargeable dual-model battery. Reproduced with permission (Yang R. et al., 2019). Copyright 2019, Royal Society of Chemistry. **(G)** Free energy of Cu–N_2 and Cu–N_4 during CO_2RR. Reproduced with permission (Zheng et al., 2019). Copyright 2019, Wiley. **(H)** Optimized adsorption configurations of Sn–Cu/Sn@SnO_x for reaction intermediates. Reproduced with permission (Ye et al., 2020). Copyright 2020, Wiley. **(I)** Optimized atomic structures for FeN_4, FeN_3, and FeN_3V embedded on the graphene layer. Reproduced with permission (Wang T. et al., 2020). Copyright 2020, Wiley. **(J)** InZnO@C. Reproduced with permission (Teng et al., 2021). Copyright 2021, Royal Society of Chemistry. **(K)** Self-driven CO production system. Reproduced with permission (Gao et al., 2021a). Copyright 2021, Royal Society of Chemistry. **(L)** N-doped ordered mesoporous carbon (NOMC). Reproduced with permission (Gao et al., 2021b). Copyright 2021, Wiley. **(M)** Sn/SnO_2@NC. Reproduced with permission (Xue Teng et al., 2021). Copyright 2021, The Core Journal of China. **(N)** Optimized Zn-N_4 and Zn-N_{3+1} structures. Reproduced with permission (Chen J. et al., 2022). Copyright 2022, Wiley. **(O)** Charge density differences maps of V-$CuInSe_2$. Reproduced with permission (Wang Y.-X. et al., 2022). Copyright 2020, Wiley. **(P)** Fe-SA/BNC. Reproduced with permission (Liu et al., 2022c). Copyright 2022, Elsevier. **(Q)** Bi clusters (BiC) deposited on hollow carbon spheres (BiC/HCS). Reproduced with permission (Yang M. et al., 2022). Copyright 2022, Elsevier.

batteries, metal–CO_2 batteries possess a higher specific capacity and energy density (Xiang Li et al., 2016; Qiao et al., 2017; Hu et al., 2019). For example, the energy density of a lithium–carbon dioxide (Li-CO_2) battery is as high as 1876 Wh kg^{-1} (Zhang et al., 2017; Cai et al., 2018), approximately five times that of a lithium-ion (Li-ion) battery (387 Wh kg^{-1} (Khurram et al., 2018; Wu et al., 2021)). However, an alkali metal (Li, Na, and K)–CO_2 battery using a toxic organic electrolyte is not environmentally friendly, and their solid products from carbon dioxide reduction (CO_2RR) are chemically inert, resulting in over-accumulation and substances not subjectable to decomposition (Xie and Wang, 2019; Mu et al., 2020). Furthermore, the slow kinetics during the electrochemical process and thermodynamic instability hinder their application. For other metal–CO_2 batteries with aqueous electrolytes, including Mg–CO_2 and Al–CO_2 batteries, their theoretical capacity densities are 6815 and 8076 Wh kg^{-1} (Ma et al., 2018), respectively, higher than that of Zn–CO_2 units (984 Wh kg^{-1}) (Aslam et al., 2023). However, the products of these metal–CO_2 batteries are all metal carbonates and carbon, which cannot generate other value-added chemicals. Zinc metal reserves are abundant, and the price is low. In the derived Zn-gas batteries, Zn–CO_2 batteries show no obvious advantages in energy density compared to Zn-air (1353 Wh kg^{-1}) or Zn-O_2 batteries but pose significant importance to CO_2 utilization and conversion (Zhou et al., 2021). Relying on environment-friendly, higher safety and wider products, the Zn–CO_2 battery is expected to be an ideal substitute for other metal batteries.

Based on its significant contribution to carbon neutrality (Chu et al., 2016; Ahmadiparidari et al., 2019; Eskezia Ayalew, 2021) and superiority in metal–gas batteries, the groundbreaking work of Zn–CO_2 batteries is exhibited in Figure 1. Aqueous Zn–CO_2 batteries originated from solar-powered CO_2 splitting batteries and later developed into a rechargeable unit, subsequently to a dual-model and self-driven system, toward the extent of a reversible one. Nevertheless, the research on aqueous Zn–CO_2 batteries is still in its infancy, and certain problems should be overcome: 1) the lack of effectively active catalysts with high selectivity leads to limited discharge products, mainly generating CO and formate, while rarely HCOOH or even less of other high value-added products (such as methanol, ethanol, and ethylene), causing the discharge–charge shuttle to be irreversible and potential application to be confined (Wang H. F. et al., 2020; Chen Y. et al., 2021). 2) The lack of stable catalytic behavior in the electrolyte environments. Most rechargeable Zn–CO_2 batteries couple CO_2RR and the oxygen evolution reaction (OER), in which CO_2RR preferably proceeds in acidic/neutral solutions and OER favors basic environments, presenting a significant challenge to balance cathodic reduction and oxidation behavior (Guo Y. et al., 2022), while a completely reversible Zn–CO_2 battery accompanied by CO_2RR and formic acid

TABLE 1 Summary of recent reports about the cathode in aqueous Zn–CO_2 batteries.

Cathode	Reactions for the cathode	Discharge products	Catholyte	Discharge–charge or O_{CV}(V)	Power density (mW cm^{-2})	Stability (N (O_{time} h)/$C_{density}$ (mA cm^{-2})	FE (%)
NOMC (Gao et al., 2021b)	CO_2RR/OER	CO_2	0.8 M $KHCO_3$	0.48/2.58	0.7	300 (100)/1.0	100
FC (Xie et al., 2018b)	CO_2RR/OER	CO	0.1 M $KHCO_3$	——	——	——	93
K-defect-C (Ling et al., 2022)	CO_2RR/OER	CO	0.8 M $KHCO_3$	——	——	200/1.5	99
SiNC (Ghausi et al., 2018)	CO_2RR/OER	CO	0.1 M $KHCO_3$	——	——	——	94
3D Pd NSs (Xie et al., 2018a)	CO_2RR/FAOR	HCOOH	1.0 M NaCl	0.78/0.96	——	100 (33)/0.56	90
Coralloid Au (Gao et al., 2021a)	CO_2RR/OER	CO	0.5 M $KHCO_3$	0.45/2.8	0.7	68 h/1.0	94.2
Ir@Au (Wang et al., 2019)	CO_2RR/OER	CO	0.8 M $KHCO_3$	0.74/2.25	——	90 (30)/5.0	90
s-SnLi (Yan et al., 2021)	CO_2RR/OER	Formate	6.0 M KOH, 0.02 M $Zn(Ac)_2$	——	1.24	>800 (85)/0.5	92
BiO_2 NSs (Tan et al., 2022)	CO_2RR/OER	Formate	1.0 M $KHCO_3$	——	2.33	300 (100)/4.5	99.1
v-$CuInSe_2$ (Wang et al., 2022b)	CO_2RR/OER	CO	0.5 M $KHCO_3$	0.55/2.4	——	>70 (40)/0.5	91
Cu-N_2/GN NSs (Zheng et al., 2019)	CO_2RR/OER	CO	0.5 M $KHCO_3$	0.7/2.4	0.62	120 (40)/1.0	64
s-PdNi (Hao et al., 2022)	CO_2RR/OER	CO	0.1 M $KHCO_3$	0.86/1.5	1.95	35 h/1.2	92.6
Bi-D (Wang et al., 2022b)	CO_2RR/OER	Formate	2.0 M $KHCO_3$ + 0.02 M $HCOO^-$	1.3 (O_{CV})	1.16	66 (22)/5.0	93.9
Bi_2O_3 NTs (Gong et al., 2019)	CO_2RR/OER	Formate	1.0 M $KHCO_3$	1.1 (O_{CV})	1.43	120 (20)/5.0	92.7
BiC/HCS(Yang et al., 2022a)	CO_2RR/OER	Formate	0.8 M $KHCO_3$	0.94 (O_{CV})	7.2 ± 0.5	200 (60)/1.0	97
Sn/SnO_2@NC (Xue Teng et al., 2021)	CO_2RR/OER	Formate	0.8 M $KHCO_3$	0.4/2.25	0.9	174 (29)/1.5	81
SnO_2/MXene (Han et al., 2022a)	CO_2RR/OER	Formate	0.1 M $KHCO_3$	0.83 (O_{CV})	4.28	60 h/2.0	94
ZnTe/ZnO@C (Teng et al., 2022)	CO_2RR/OER	Formate	0.8 M $KHCO_3$	1.35 (O_{CV})	0.93	36 (108)/1.0	86
In/ZnO@C NCs (Teng et al., 2021)	CO_2RR/OER	Formate	0.5 M $KHCO_3$	1.35 (O_{CV})	1.32	153 (51)/1.0	90
Fe_1-Ni_1-N-C (Jiao et al., 2021)	CO_2RR/OER	CO	0.8 M $KHCO_3$	——	——	15 h/1.1	96.2
BiPbC (Gao et al., 2022a)	CO_2RR/FAOR	HCOOH	0.1 M $KHCO_3$ + 0.1 M HCOONa	1.2 (O_{CV})	0.42	45 h/0.5	52.6
Fe-P@NCPs (Liu et al., 2022d)	CO_2RR/OER	CO	1.0 M $KHCO_3$	0.55/2.33	0.85	500 (7 days)/0.5	95
Cu_3P/C (Peng et al., 2019)	CO_2RR/OER	CO	0.1 M $KHCO_3$	1.5 (O_{CV})	2.6	——	47
Ni/PNG (Yang et al., 2019c)	CO_2RR/OER	CO	3.0 M $KHCO_3$ + 1.5 M KCl	0.47/2.58	0.28	215 (36)/0.2	66

(Continued on following page)

TABLE 1 (*Continued*) **Summary of recent reports about the cathode in aqueous Zn–CO_2 batteries.**

Cathode	Reactions for the cathode	Discharge products	Catholyte	Discharge–charge or O_{CV}(V)	Power density (mW cm^{-2})	Stability (N (O_{time} h)/$C_{density}$ (mA cm^{-2})	FE (%)
Ni-N_3-C (Zhang et al., 2021b)	CO_2RR/OER	CO	0.8 M $KHCO_3$	0.41/2.4	——	100/2.0	95.6
Fe_1NC/S_1-1000 (Wang et al., 2020c)	CO_2RR/OER	CO	0.8 M $KHCO_3$	0.73 (O_{CV})	0.6	72 (25)/0.5	95.6
Fe-N_5/DPCF (Li et al., 2022b)	CO2RR/OER	CO	0.8 M KHCO3	1.3 (O_{CV})	——	75 (25)/0.5	90
Fe-SA/BNC (Liu et al., 2022c)	CO_2RR/OER	CO	0.8 M $KHCO_3$	0.51/2.33	1.18	80 (27)/-1.0	94
CoPc@DNHCS-8 (Gong et al., 2022)	CO_2RR/OER	CO	0.5 M $NaHCO_3$	0.75 (O_{CV})	1.02	40 h/1.0	95.7
Zn-N_{3+1} (Chen et al., 2022a)	CO_2RR/OER	CO	0.5 M $KHCO_3$	0.77 (O_{CV})	1.8	100 (26)/1.5	95
Ni-N_x-2D/NPC (Zeng et al., 2021)	CO_2RR/OER	CO	1.0 M $KHCO_3$	0.3/2.5	——	50 h/0.25	95

oxidation reaction (FAOR) is built in neutral or slightly acidic electrolytes, triggering electrochemical corrosion or other undesired side reactions and significantly shortening the battery life. 3) The high overpotential and low current density (≤10 mA cm^{-2}) severely compromise the power and energy density, where increasing energy consumption and poor long-term reversibility pose a significant obstacle toward practical application. These mentioned problems of a Zn–CO_2 battery are mainly attributed to the high stability of the C=O bond (dissociation energy as high as 806 kJ mol^{-1}) in CO_2 (Zhou and Sun, 2017; Kim et al., 2020), finite product types, poor selectivity in CO_2RR, and low electrochemical activity in the cathodic oxidation reaction. Indeed, it is tricky to obtain efficient long-term reversible cycles without effective catalysts (Hao et al., 2020; Hao et al., 2021). Moreover, the aqueous electrolytes present low operation potential and anode instability (like Zn self-corrosion or dendrite), resulting also in limited running cycles, but these topics are beyond our discussion in this review.

Therefore, it is crucial to design both effective and chemical/electrochemical stable catalysts to solve the aforementioned problems, tackling competitive adsorption–desorption between *COOH/*OCHO, *COH/*CO, *OH/*OOH, or *H in the catalytic process for the target products (Huang et al., 2019). Despite many updated papers on cathode materials (Table 1) for aqueous Zn–CO_2 batteries, a systematic summary has rarely been reported (Wu et al., 2021), and even less is known about the principles of designing efficient catalysts. Herein, this review summarizes the structure and mechanism of Zn–CO_2 battery and discusses the research progress and existing problems of cathode materials, and, more importantly design strategies and preparation methods for efficient cathode catalysts are proposed, centering on catalyst structure with adsorption performance of intermediate products, eventually highlighting the opportunities and challenges for high-performance Zn–CO_2 batteries, which enables to enlighten the future development of the next-generation energy storage system.

The results were obtained from the data by providing directly from literature or estimating from the given information. NOTE:

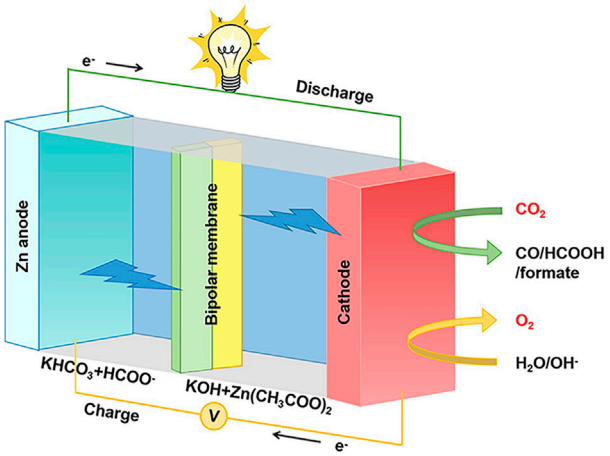

FIGURE 2
Schematic diagram of rechargeable Zn–CO_2 battery.

Dis-char means discharge–charge plateau. O_{cv} means open-circuit voltage. O_{time} means operation time. $C_{density}$ means current density. For better performance evaluation, the data in red, blue, and green represent excellent, good, and average, respectively.

2 Structure and reaction mechanism of Zn–CO_2 battery

2.1 Battery structure

The Zn–CO_2 battery typically consists of a catalyst cathode, Zn sheet anode, electrolyte, and diaphragm seen in Figure 2. Its uniqueness is the electrolyte, which is divided into two parts: the anode counterpart utilizes alkaline KOH and $Zn(CH_3COO)_2$

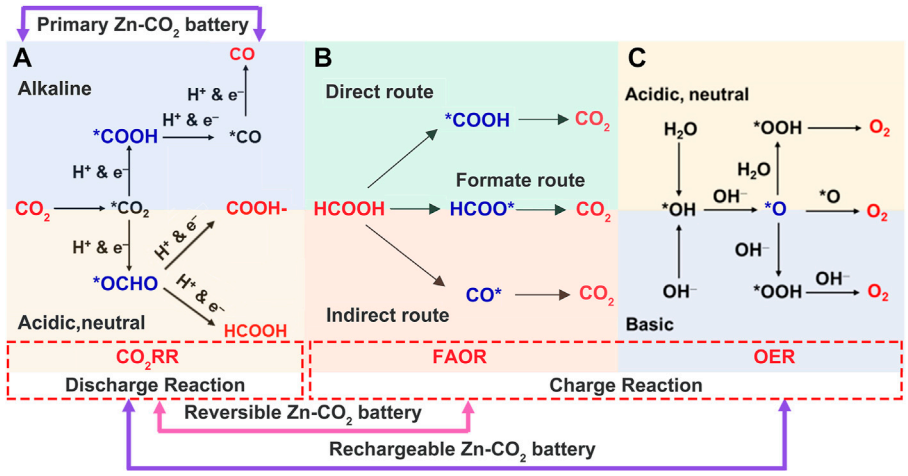

FIGURE 3
Cathodic reaction mechanism. **(A)** Possible pathways of aqueous CO_2RR with diverse products. Possible pathways of **(B)** FAOR in direct, formate, and indirect routes and **(C)** OER in acidic (or neutral) and basic electrolytes. Reproduced with permission (Xie et al., 2019). Copyright 2019, Wiley. * represents the active site. The generation of intermediate (represented in blue) is the rate-determining step.

mixture solution, while the cathode counterpart uses near-neutral $KHCO_3$ solution, and sometimes, buffer solution $HCOO^-$ is added (Asokan et al., 2020). Bipolar membranes are necessary to separate the electrodes, maintaining the pH and avoiding cross-contamination (Xie et al., 2018a).

2.2 Reaction mechanism

Based on the Frontier research progress of Zn–CO_2 batteries, we discuss both anodic and cathodic reaction mechanisms and highlight the cathodic CO_2 electrochemical reduction and opposite evolution mechanisms in alkaline and neutral electrolyte conditions.

2.2.1 Anodic reaction mechanism

The anodic reactions are based on Zn/Zn^{2+} redox couple, and the Zn^{2+} state is affected by the electrolyte's pH shown as follows. In near-neutral electrolytes, Zn^{2+} exists as the charge carrier, while in alkaline solutions, Zn^{2+} initially appears as $Zn(OH)_4^{2-}$ and is further dehydrated to ZnO (Zhong et al., 2020).

In the neutral electrolyte: E^{θ} (Zn/Zn^{2+}) = −0.76 V vs. SHE, where E^{θ} means the standard reduction potential

$$Zn \leftrightarrow Zn^{2+} + 2e^{-}. \quad (1)$$

In the alkaline electrolyte: E^{θ} (Zn/ZnO) = −1.22 V vs. SHE

$$Zn + 4OH^{-} \leftrightarrow Zn(OH)_4^{2-} + 2e^{-}. \quad (2)$$

$$Zn(OH)_4^{2-} \leftrightarrow ZnO + 2OH^{-} + H_2O. \quad (3)$$

2.2.2 Cathodic reaction mechanism

CO_2RR mechanism: When Zn–CO_2 batteries discharge, CO_2RR occurs on the gas–liquid–solid three-phase interface, and this complex process involves the adsorption and dissociation of CO_2 together with the transfer of multiple protons and electrons (Li et al., 2017; Yang et al., 2018). CO_2RR products are mainly present as HCOOH/formate and CO through different routes in the adsorption model on the catalytic site. The former tends to adsorb at the O end (*OCHO) to present HCOOH in near-neutral electrolytes and transit to formate in alkaline environments (Han et al., 2018), while the latter adsorbs at the C end (*COOH), as shown in Figure 3A.

HCOOH in the neutral electrolyte:

$$CO_2 + 2H^{+} + 2e^{-} \rightarrow HCOOH. \quad (4)$$

Formate in the alkaline electrolyte:

$$CO_2 + 2e^{-} + H_2O \rightarrow HCOO^{-} + OH^{-}. \quad (5)$$

CO in the alkaline electrolyte:

$$CO_2 + 2H^{+} + 2e^{-} \rightarrow CO + H_2O. \quad (6)$$

Relying on the reversibility of a discharge–recharge reaction, the Zn–CO_2 secondary battery is classified into two types: the reversible battery covering the HCOOH product and FAOR charge process and the rechargeable one generating CO or $HCOO^-$ discharge products and coupling OER (simplified as Zn–CO_2 battery) (Wang F. et al., 2021). We discuss the charge mechanism as follows.

FAOR mechanism: The reversible Zn–CO_2 battery forms a closed loop between CO_2 and HCOOH (El Sawy and Pickup, 2016; Xiong et al., 2020; Liang M. et al., 2021). FAOR generally occurs in the direct, indirect, or formate pathways (Wang et al., 2004; Zhu et al., 2021a), as seen in Figure 3B. The direct route follows the dehydrogenation of HCOOH with the C-H bond breaking and release of CO_2, which occur quickly and effectively under low potential. As for the indirect route, the initial step is dehydration with C-O and C-H bonds breaking, and the adsorbed CO (CO*) is subsequently oxidized to CO_2 at high potential. The residual CO* covers active sites and seriously represses the direct route, leading to

TABLE 2 Reaction mechanisms of the Zn–CO_2 battery.

Battery Type	Discharge reaction mechanism	Charge reaction mechanism
Primary Zn-CO_2 battery	$CO_2(g) + 2H^+ + Zn + 4OH^- \rightarrow Zn(OH)_4^{2-} + CO(g) + H_2O$	-
Rechargeable Zn-CO_2 battery	$CO_2(g) + 2H^+ + Zn + 4OH^- \rightarrow Zn(OH)_4^{2-} + CO(g) + H_2O$ **or** $CO_2(g) + H^+ + Zn + 4OH^- \rightarrow Zn(OH)_4^{2-} + HCOO^-$	$2Zn(OH)_4^{2-} + 2H_2O \rightarrow O_2(g) + 2Zn + 4OH^- + 4H^+$
Reversible Zn-CO_2 battery	$CO_2(g) + Zn + 4OH^- + 2H^+ \leftrightarrow Zn(OH)_4^{2-} + HCOOH(aq)$	

catalyst poisoning or even inactivation (Calderón-Cárdenas et al., 2021). Different from the breaking sequence of the direct route, the formate route first breaks the O-H bond of HCOOH to HCOO* (i.e., *OCHO) and further dehydrogenates to CO_2, requiring less binding energy than the aforementioned two paths, thus occurring at even lower potential (Xiong et al., 2020).

Direct route:

$$HCOOH \rightarrow COOH^* + H^+ + e^- \rightarrow CO_2 + 2H^+ + 2e^-. \quad (7)$$

Indirect route:

$$HCOOH \rightarrow CO^* + H_2O \rightarrow CO_2 + 2H^+ + 2e^-. \quad (8)$$

Formate route:

$$HCOOH \rightarrow HCOO^* + H^+ + e^- \rightarrow CO_2 + 2H^+ + 2e^-. \quad (9)$$

To date, CO_2RR products in the battery are mostly CO or formate and catalysts with high FAOR activity are rarely reported. The reversible Zn–CO_2 batteries following the formate path are only achieved under bifunctional catalysts of porous Pd nanosheets (Xie et al., 2018a) and PdBi alloy (Gao S. et al., 2022).

OER mechanism: O_2 is generated from H_2O molecules in acidic electrolytes or from -OH groups in alkaline media during the OER, as shown in Figure 3C (Suen et al., 2017; Xie et al., 2019). Its symbiotic hydrogen evolution reaction (HER) seriously affects the battery's Coulombic efficiency and should be inhibited.

$$H_2O \rightarrow \frac{1}{2}O_2 + 2H^+ + 2e^-, E_{c2} = 0.80V. \quad (10)$$

To sum up, the reaction mechanisms of the Zn–CO_2 battery are listed in Table 2. The continuous exploration of mechanisms enlightens the direction of efficient catalysts (Wang K. et al., 2020; Wang F. et al., 2021).

3 Cathode catalysts

The catalytic properties and electrolyte environment play a significant role in the electrochemical mechanism, influencing product state and reaction rate and ultimately determining its battery performance (Wang J. et al., 2021). Cathode catalysts (as the core component) are divided into three categories in this review: carbon-based metal-free catalysts, metal-based catalysts, and metal–carbon composites. When the battery discharges, CO_2 is mostly reduced to CO and formate and rarely to HCOOH, depending on reaction intermediates. Specifically, accelerating the formation of *COOH tends to produce CO while reducing the reaction energy barrier of *OCHO, which promotes the generation of HCOOH in near-neutral electrolytes and formate in alkaline electrolytes (Xie et al., 2019). In the opposite charge process, it requires cathodes to show pertinent desorption catalysis of *COOH/HCOO*/CO* in FAOR or *OH/*OOH in the OER. The adsorption energy of intermediates reflects the catalytic activity and is influenced by the electronic structure and chemical environment of the catalytic sites (Selvakumaran et al., 2019; Peng et al., 2022b).

3.1 Carbon-based catalyst

This catalyst has the advantages of high conductivity, large specific surface area, superior stability, and low costs and involves carbon nanotubes, graphene, and other analogs (Lankone et al., 2017; Yu et al., 2020; Zhao et al., 2020; Chen B. et al., 2021). The catalytic performance is further regulated via doping N, F, Si, or P heteroatoms into the electronic structure and introduces defects (Xue et al., 2019; Wang C. et al., 2021; Gao Y. et al., 2022; Wang J. et al., 2022). Generally, the doped heteroatoms with strong electronegativity facilitate the combination with positively charged *COOH intermediates (Shi et al., 2021; Sawant et al., 2022; Thakur et al., 2022). N-doped carbon materials are widely used in this field. As reported in literature, N-doped ordered mesoporous carbon (NOMC) (Gao et al., 2021b) (Figures 4A, B) using the SBA-15 template is prepared via the pyrolytic-etching method, possessing ultra-high specific surface area, highly exposed N-C sites to promote the transport and storage of reactants/intermediates (Shakeri et al., 2021). The Faraday efficiency of the CO product (FE_{CO}) on NOMC is close to 100% at a low overpotential of 0.36 V, and a Zn–CO_2 battery assembled with the NOMC cathode achieves long, stable cycles of 300 (100 h) even at 1.0 mA cm^{-2} (Figures 4C, D), indicating high catalytic performance and super stability. The presence of more electronegative F atoms induces positrons and arouses asymmetric spins, thereby rearranging the electron density of adjacent atoms (Wang G.-D. et al., 2021).

A few F atoms were adopted into carbon matrices forming F-doped carbon (FC) (Figures 4E–H) by the one-step pyrolysis method, and the FC catalyst was applied in Zn–CO_2 for the first time (Xie et al., 2018b). Through density functional theory (DFT) calculation (Figures 4I–K), it was shown that *COOH is inclined to adsorb on the fourth C atom next to the CF_2 bond with the lowest Gibbs free energy (ΔG) of 0.64 eV rather than the F-free doped C atom. Simultaneously, it endows the adjacent C atoms with higher positive charge density and asymmetric spin sites, effectively inhibiting the HER with strong binding ability to H*. As a result, its FE_{CO} is increased to 89.6%, and the assembled solar-driven CO_2

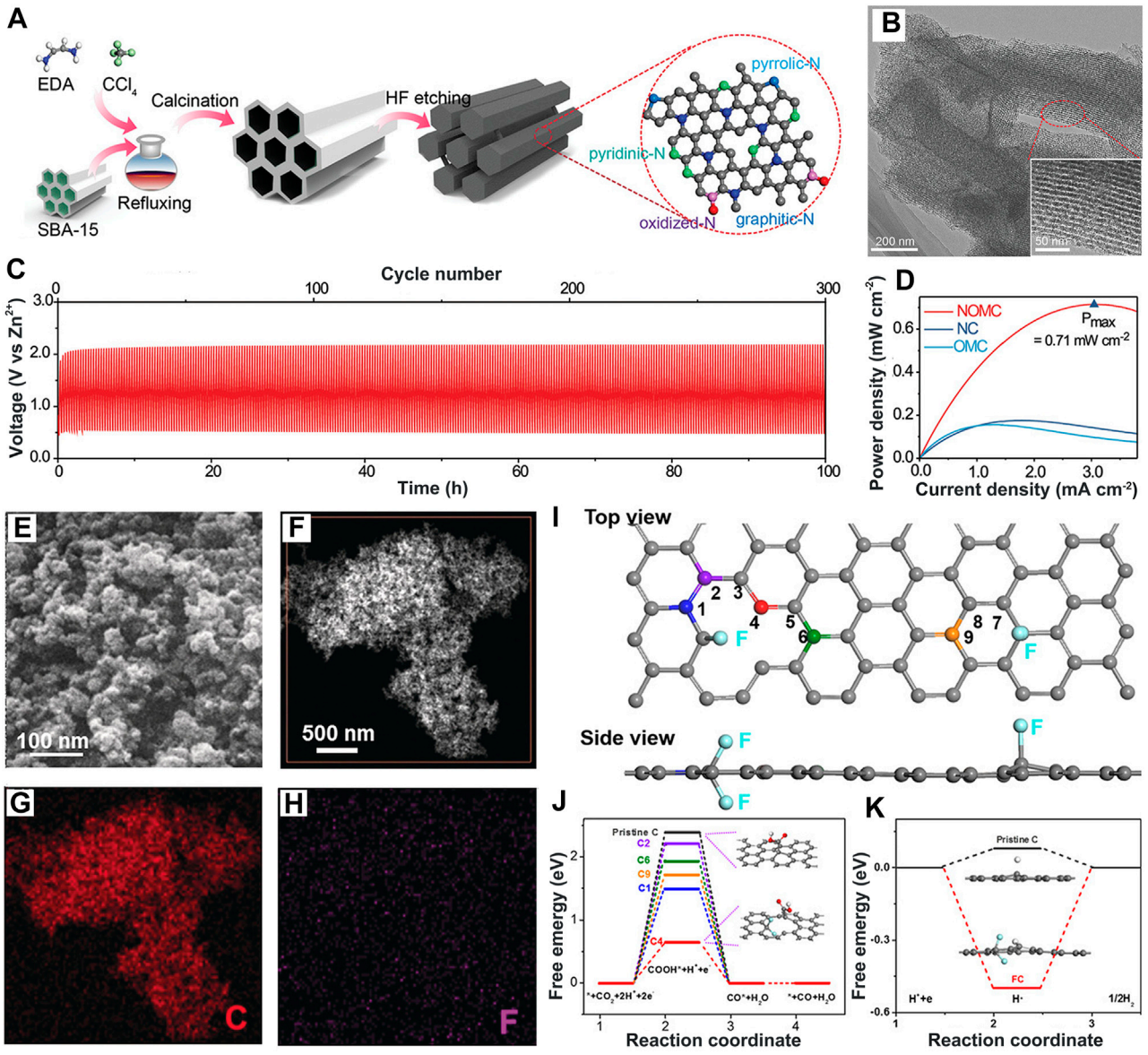

FIGURE 4
(A) Schematic illustration and **(B)** TEM image of NOMC. **(C)** Stability and **(D)** power density curves of Zn–CO_2 battery with NOMC. Reproduced with permission (Gao et al., 2021b). Copyright 2021, Wiley. **(E,F)** SEM and HAADF images of FC and **(G,H)** related EDS mapping. **(I)** Top and side views of the DFT model for FC. Gray atom: C; other colorful atoms: C calculated as active sites. **(J)** Free energy diagram of CO_2RR to CO on FC. **(K)** Schematic of the CO_2RR pathway on FC. Reproduced with permission (Xie et al., 2018b). Copyright 2018, Wiley.

battery achieves 13.6% photoelectric conversion efficiency, higher than that of SiNC materials (Ghausi et al., 2018) (12.5%). Such energy conversion–storage Zn–CO_2 self-powered devices conform to the trends in the development of self-powered integrated devices.

In addition to heteroatom doping, the construction of intrinsic carbon defects causes charge delocalization, activating carbon atoms at defect sites for better catalytic properties. A defect-rich porous carbon (K-defect-C-1100) was synthesized by a K^+-assisted strategy (Ling et al., 2022) and has 12-vacancy-type defects (V_{12}) (Figures 5A–D). Its negative potential V_{12} defect attracts electrophilic CO_2 molecules and renders the battery high FE_{CO} to 99% (Figure 5E) in a wide discharge potential range with excellent cyclic stability of about 200 cycles.

Though electron delocalization is induced into carbon-based materials, the influence on the inertia of molecular activation is finite, which hardly meets application requirements.

3.2 Metal-based catalysts

Metal-based catalysts are generally composed of metal or alloy nanoparticles and metal compounds. Noble metal-based catalysts such as Au, Ru, Pd, and Ir have excellent catalytic properties, providing good acid and alkali resistance (Li D. et al., 2022; Zhao D. et al., 2022; Kang T. et al., 2022; Huang et al., 2022); the exposure states of active sites are easily made compatible via structure design

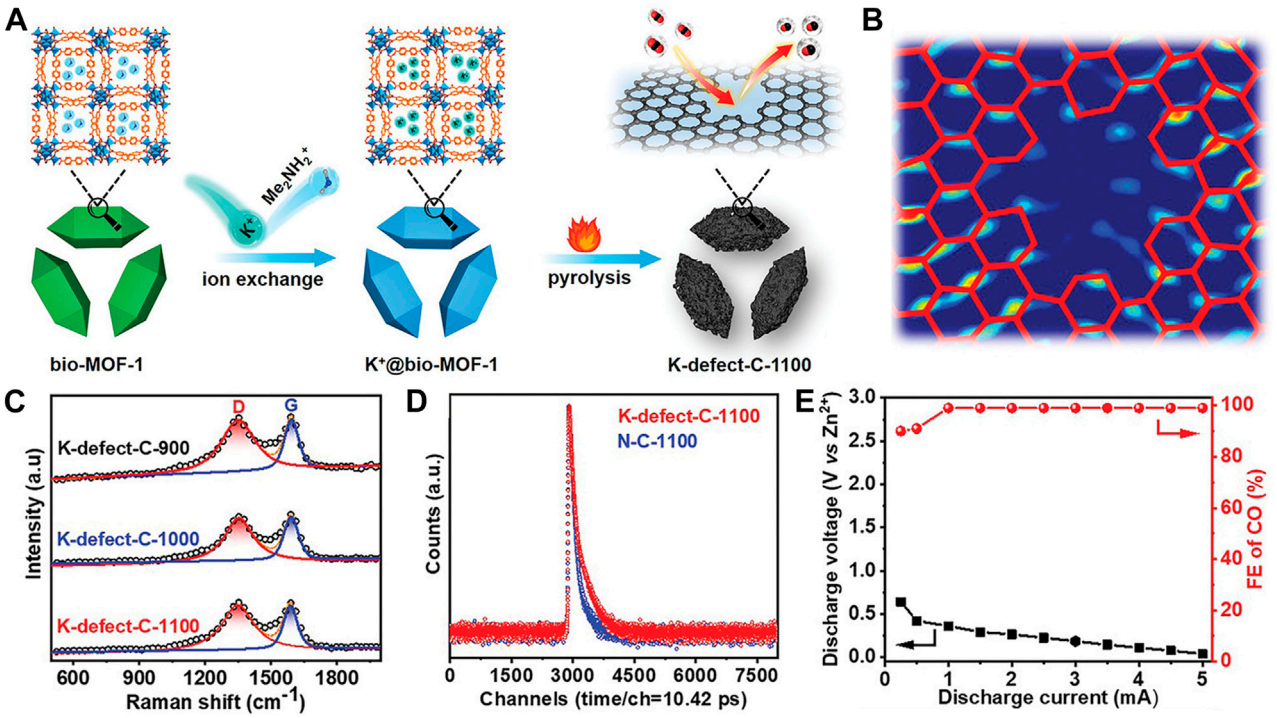

FIGURE 5
(A) Schematic illustration of K-defect-C-1100 preparation. **(B)** HAADF-STEM image of K-defect-C-1100 after fast Fourier transformation filtering. **(C)** Raman spectra and **(D)** PALS spectra of K-defect-C-1100. **(E)** Discharge voltages and the corresponding FE_{CO} profiles at different current densities. Reproduced with permission (Ling et al., 2022). Copyright 2022, Wiley.

and mass transfer capacity (Sui et al., 2021). Additionally, the catalyst's lattice structure and charge distribution are evolved by introducing other metal or non-metallic atoms, which optimizes the interaction between the catalyst and intermediates, inhibits possible side reactions, and allows an elevation of the product selectivity (Feng et al., 2021).

As reported, Xie et al. (2018a) prepared porous three-dimensional interconnected Pd nanosheets (3D Pd NSs) with a rich pore structure, large specific surface area, sufficient active sites by electrodeposition (which adsorbs the *OCHO intermediate with high selectivity), and presents a good reversibility in conversion between CO_2 and HCOOH under low potential. The assembled reversible Zn–CO_2 battery steadily runs for more than 100 cycles (33 h), achieves a 788 Wh kg^{-1} discharge capacity, and shows an energy efficiency of 81.2%. Gao et al. (2021a) prepared coral-like Au catalyst with an irregular surface and initiated a self-driven CO production device that is co-assembled by a Zn–CO_2 battery and H-type CO_2 electrolyzer for the first time. *COOH is easily adsorbed on Au (111), with a lower reaction energy barrier (ΔG = 1.16 eV) than that in the common environment (ΔG = 1.27 eV). Unlike single metals, bimetal composites do achieve enhanced catalytic performance under the strong synergistic effect. Wang et al. (2019) built a dendritic 3D Ir@Au bifunctional catalyst and constructed a Zn–CO_2 battery simulating the two-step plant photosynthesis to achieve CO_2 fixation and H_2O oxidation, which equably circulates for 30 h at 5 mA cm^{-2}.

Although noble metals exhibit outstanding catalysis in Zn–CO_2 batteries, their commercial application is restrained by high prices and low reserves. Alloys and transition metals with special catalytic properties are becoming their alternatives (Yang X. et al., 2022; Gao and Zhao, 2022; Lichchhavi and Shirage, 2022). Sn is rich in resources with low toxicity. In the electrochemical reaction, the Sn alloy and Sn_2O_3 are utilized as important promoters to reduce CO_2 to C1 products (CO and HCOOH), but their poor conductivity is still an obstacle (Kang J. et al., 2022; Ansari et al., 2022). The hierarchical core-shell Sn–Cu/Sn@SnO_x (Ye et al., 2020) (Figures 6A–C) was optimized with high conductivity by an Sn/SnO_x interface. Its Sn–Cu/Sn core provides a sufficient Sn source to reconstruct the core-shell structure, thereby guaranteeing stability. Its *in situ* reconstructed Sn/SnO_x shell increases the reaction energy barrier of *H and *COOH to suppress HER and CO formation; conversely, it reduces the *OCHO binding energy, which sets a decisive step toward obtaining a high selectivity of the HCOOH product and presents a high $FE_{formate}$ (Figures 6D, E). However, its partial current density of formate ($j_{formate}$) is still lower than −0.3 A cm^{-2}, which is far from application requirements. To solve this problem, Sn is incorporated with Li (s-SnLi) (Yan et al., 2021) on the surface, which stimulates local electron rearrangement and lattice strain that correspondingly occurred on the adjacent Sn atoms, showing more negative charge (Figure 6F).

Therefore, the s-SnLi with enhanced CO_2 adsorption capacity and restricted ΔG_{*COOH} and ΔG_{*OCHO} (Figure 6G) showed both high catalysis and selectivity in reducing CO_2 to formate. Thus, $FE_{formate}$ reaches 92%, the maximum power density of 1.24 mW cm^{-2}, $j_{formate}$ is increased to −1.0 A cm^{-2}, and the Zn–CO_2 cell operates for over 800 cycles.

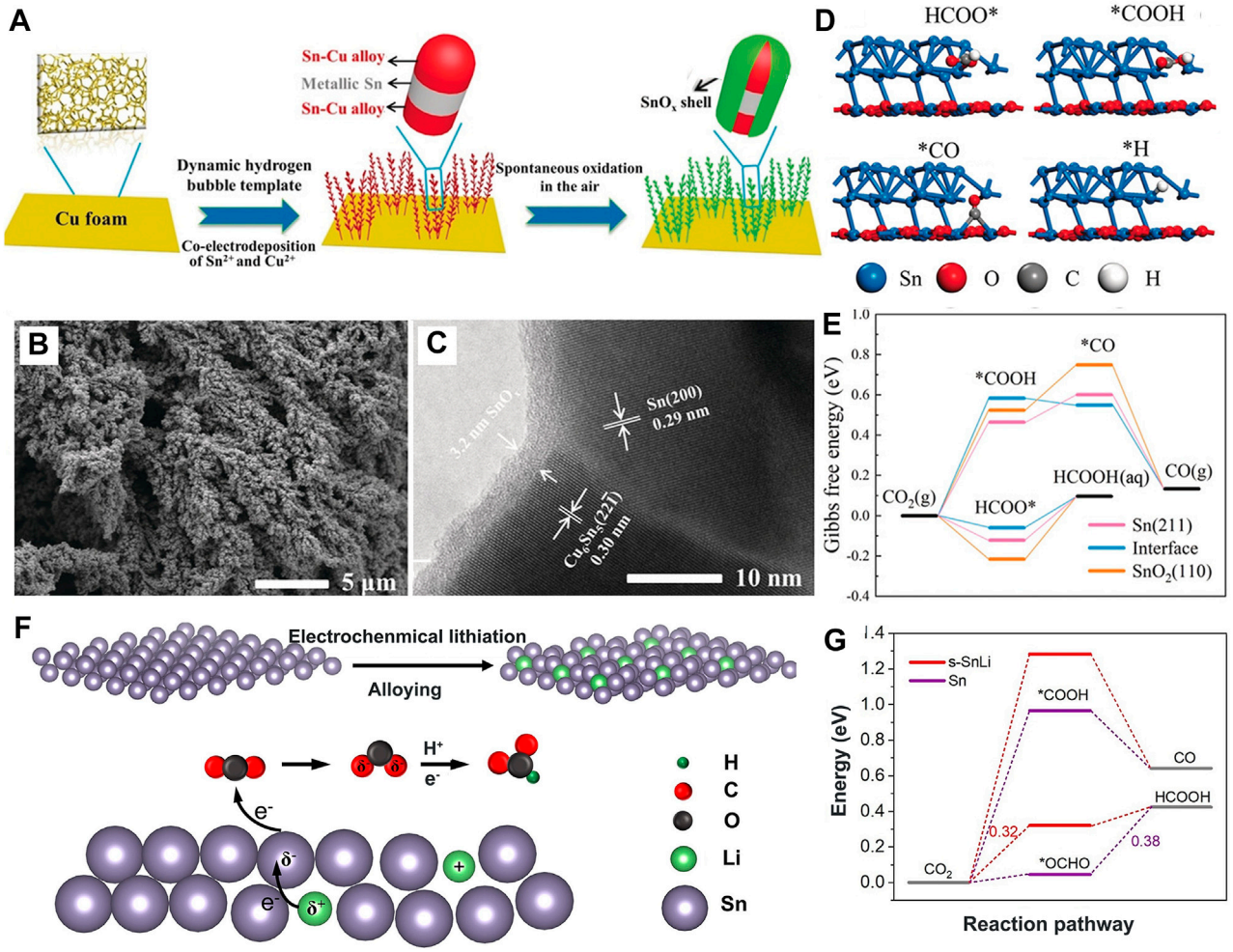

FIGURE 6
(A) Schematic illustration of Sn-Cu/Sn@SnO_x. **(B)** SEM and **(C)** HRTEM images of Sn-Cu/Sn@SnO_x. **(D)** Optimized adsorption configurations for reaction intermediates at the interface. **(E)** Gibbs free energy diagrams of **(E)** CO_2RR on the Sn/SnOx interface. Reproduced with permission (Ye et al., 2020). Copyright 2020, Wiley. **(F)** Schematic illustration of s-SnLi and catalyst mechanisms for CO_2RR to formate. **(G)** Mechanism investigations of CO_2RR to HCOOH and CO on s-SnLi. Reproduced with permission (Yan et al., 2021). Copyright 2022, Royal Society of Chemistry.

Metal oxides behave better in CO_2RR performance than metal substances, but metal self-reduction may occur in the catalytic process. BiO_{2-x} nanosheets (m-BiO_{2-x}) with rich oxygen defects (Tan et al., 2022) and favorable localization of Bi p-orbital electrons were utilized to stabilize *OCHO and suppress *H adsorption for high selectivity in CO_2-to-formate conversion. It offered a non-dopant pathway to boost electrochemical CO_2RR. Inspired by the synergetic effect of multi-metals, Tian et al. (2021) embedded SnO_2 nanoparticles on Bi_2O_3 sheets' surfaces to assemble SnO_2/Bi_2O_3 composites. Different work functions at the SnO_2/Bi_2O_3 interface induce a built-in potential, thereby promoting the interface electron transfer and improving the conductivity of SnO_2. The strong interface on SnO_2/Bi_2O_3 effectively prevents SnO_2 from electrolytic decomposition, which ensures catalyst stability and promotes CO_2 adsorption and activation. In addition, it showed the enhanced adsorption of *OCHO on Bi_2O_3 to accelerate HCOOH generation and the very strong adsorption of *H to inhibit the HER (Figures 7A, B). The bimetallic oxides integrated stability and catalytic activity, achieving a multifunctional catalyst (Guo H. et al., 2022).

Moreover, metallic selenides are an option in CO_2RR catalysts due to their low cost and unique physical and chemical properties, but their selectivity in products is poor (Hu H. et al., 2021). As reported, In_2Se_3 nanosheets reduce CO_2 to CO with an FE_{CO} of 89% (Lü et al., 2019), and $Cu_{1.63}Se_{0.33}$ reduces CO_2 to CH_3OH with an FE_{CH3OH} of only 77.6% (Yang D. et al., 2019). Both examples show that catalyst activity and product selectivity are in great demand for improvement. Bimetallic selenides v-$CuInSe_2$ (Wang Y.-X. et al., 2022) (Figure 7C) were prepared to possess the bimetallic orbital, which regulates the adsorption–desorption strength of *COOH being more conducive to CO generation and shows no stable *H adsorption sites, thereby significantly inhibiting the HER (Figure 7D). Thus, FE_{CO} was increased to 91% at −0.70 V (vs. RHE).

For metal-based catalysts, the structure and morphology of noble/transition metals are designed to avoid aggregation and self-reduction,

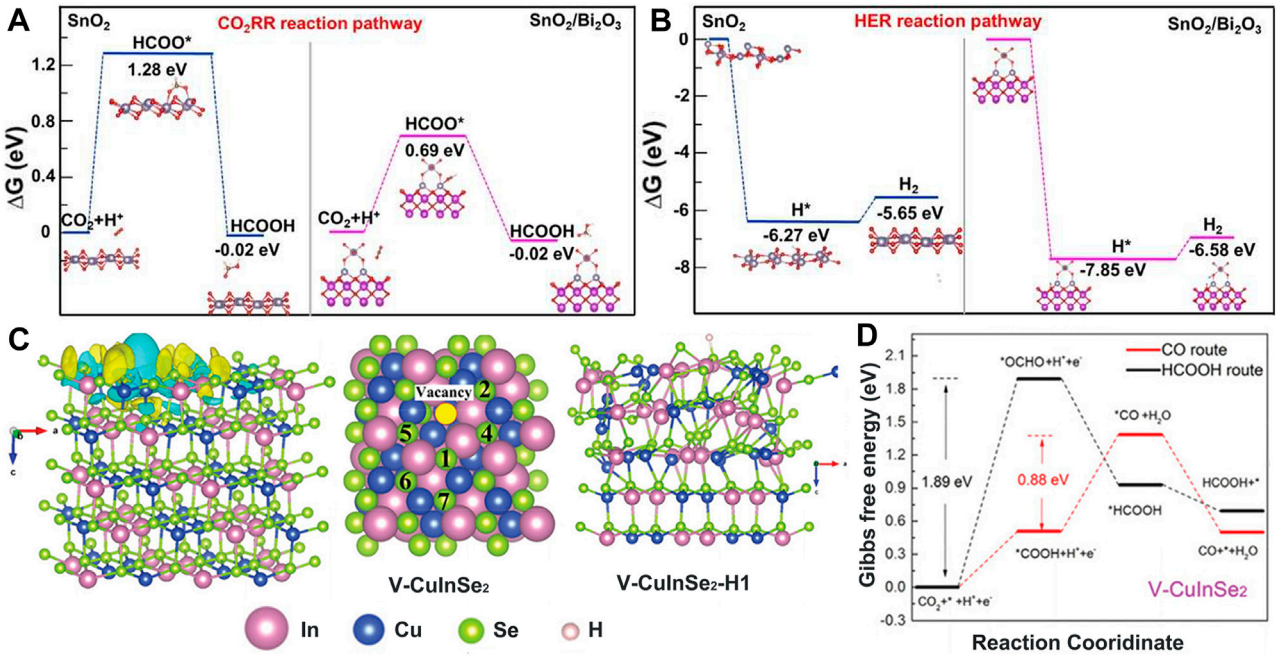

FIGURE 7
Reaction adsorption energy diagram of **(A)** CO_2RR and **(B)** HER pathways on SnO_2/Bi_2O_3. Reproduced with permission (Tian et al., 2021). Copyright 2021, Wiley. **(C)** Charge density differences maps of V-$CuInSe_2$ (yellow and blue regions represent the accumulation and depletion of electrons, respectively). **(D)** Mechanism investigations of the CO_2RR pathway on V-$CuInSe_2$. Reproduced with permission (Wang Y.-X. et al., 2022). Copyright 2022, Wiley.

where the hybridization and alloying strategy is adopted to modify the electron distribution for excellent catalytic behaviors.

3.3 Metal–carbon composite catalysts

The metal-based catalysts are prone to agglomerate, leading to a decrease in catalytic activity (Chen et al., 2022b). It is a strategy to isolate metal nanoparticles on carbon substrates (Lei et al., 2022) for catalytic performance and conductivity, thereby deriving metal-carbon catalysts. Such materials have excellent geometric structures and fully expose the specific active sites (Zhao S. N. et al., 2022). Their catalysis is not only related to the inherent properties of embedded metal and carbon frame but also regulated via the morphology and interface modification (creating defects and heterostructure) (Belotcerkovtceva et al., 2022; Cao et al., 2022; Fan et al., 2022; Su et al., 2022).

Metal Bi can enhance *OCHO adsorption and inhibit *H adsorption, but is easily oxidized due to its low melting point (Deng et al., 2020; Chhetri et al., 2022). To avoid oxidation, Bi is uniformly dispersed in a carbon layer, which creates an abundance of defects (Bi-D) (Wang J. et al., 2022), thereby showing hybrid crystalline–amorphous phases and heterojunctions, that render the $FE_{formate}$ as high as 90%; the maximum power density was 1.16 mW cm^{-2}. Bi geometry was changed into nanotubes (Bi_2O_3 NTs) that accelerated the $FE_{formate}$ higher than 92.7%, and the maximum power density was up to 1.43 mW cm^{-2} (Gong et al., 2019). In addition, Bi clusters are deposited on hollow carbon spheres to form atomic dispersed BiC/HCS (Yang M. et al., 2022), improving CO_2 adsorption capacity, increasing the FE_{CO} to 97% ± 2% (−0.6 V vs. RHE), achieving a record-breaking peak power density of 7.2 ± 0.5 mW cm^{-2}, and a cycle number of more than 200 times.

The Sn/SnO_x heterojunction presented higher catalytic activity than individual Sn, as previously mentioned. Multivalent Sn provides rich interfaces between Sn(0) and Sn(II) or Sn(IV), showing a special catalytic activity in stabilizing intermediates (Liu K. et al., 2022; Spada et al., 2022; Zhang et al., 2022). The Sn/SnO_2 heterojunction was uniformly decorated on highly conductive N-doped carbon networks to construct Sn/SnO_2@NC (Xue Teng et al., 2021). The $FE_{formate}$ is increased to 81%, the peak power density of the assembled battery reaches 0.9 mW cm^{-2}, and the open-circuit voltage is 1.35 V. Furthermore, the carbon network was replaced by potential two-dimensional materials. Low-dimensional SnO_2 quantum dots were spread among ultrathin $Ti_3C_2T_x$ MXene nanosheets (SnO_2/MXene) (Han L. et al., 2022) to reduce the reaction energy of CO_2 hydrogenation to formate. This is carried out by destabilizing water and water dissociation in order to increase the surface coverage of *H and raise a new situation of electrochemical CO_2-to-formate.

Similarly, bimetal or multimetal catalysts are rooted into carbon substrates to play a synergetic role via inducing geometric or electronic reconstructions (Zhang N. et al., 2021; Kong et al., 2022). For example, the In metal can reduce CO_2 to formate, but is faced with many obstacles such as low $j_{formate}$, poor stability, and limited coordination ability (Dong et al., 2018; Raknual et al., 2021).

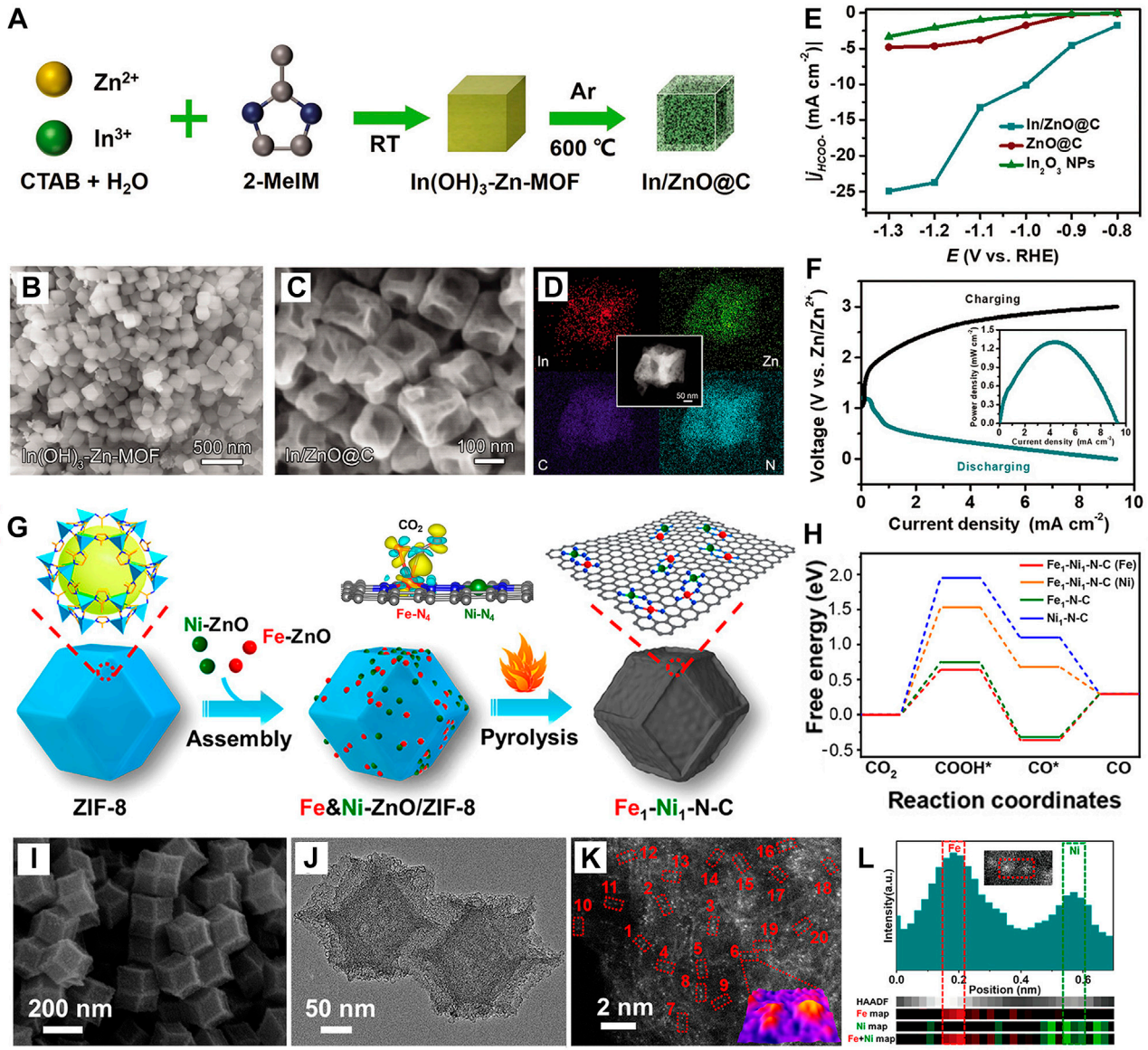

FIGURE 8
(A) Schematic illustrations of In/ZnO@C. SEM images of **(B)** $In(OH)_3$-Zn-MOF precursors and **(C)** In/ZnO@C. **(D)** DEX mapping of In/ZnO@C. **(E)** $j_{formate}$ in CO_2-saturated 0.5 M $KHCO_3$ solutions. **(F)** Galvanostatic charge–discharge and power density curves of Zn–CO_2 battery shown in the inset. Reproduced with permission (Teng et al., 2021). Copyright 2021, Royal Society of Chemistry. **(G)** Schematic illustrations of Fe_1-Ni_1-N-C. **(H)** Free energy diagrams of CO_2RR on Fe_1-Ni_1-N-C. **(I)** SEM and **(J)** TEM images of Fe_1-Ni_1-N-C. **(K)** Aberration-corrected HAADF-STEM observation for Fe_1-Ni_1-N-C (inset: 3D atom-overlapping the Gaussian-function fitting map of region 6 in panel **(K)**. **(L)** HAADF-STEM intensity profile and atomic resolution EELS mapping of the Fe–Ni pair. Reproduced with permission (Jiao et al., 2021). Copyright 2021, Wiley.

To resolve these problems, In is fixed into Zn-MOF derivatives to prepare In/ZnO@C hollow nanocubes (Teng et al., 2021) (Figures 8A–D), thereby adjusting the adsorption of *OCHO on Zn catalytic sites and improving the product selectivity. Under the hollow nanocube framework, the synergetic effect of both Zn and In makes $j_{formate}$ as high as 23.5 mA cm^{-2}, $FE_{formate}$ increases to 90% at a potential of −1.2 V (vs. RHE), long cycles of 153 (51 h) at the current density of 1 mA cm^{-2}, and the peak power density of a Zn–CO_2 battery is improved to 1.32 mW cm^{-2} (Figures 8E, F). Simultaneously, Fe and Ni nanoparticles are introduced into ZIF to synthesize Fe_1–Ni_1–N–C (Jiao et al., 2021) (Figure 6G), existing as Fe-N_4 and Ni-N_4 forms. Fe and Ni monoatomic pairs play a synergistic effect, where Ni atoms activate the adjacent Fe to increase the electron density between Fe and CO_2 while reducing the free energy of *COOH (Figures 8H–L); thus, its FE_{CO} reaches 96.2% at −0.5 V. Furthermore, a bifunctional PdBi alloy anchored on the carbon substrate (BiPdC) (Gao S. et al., 2022) was fabricated via doping Pd into Bi-based MOF (CAU-17) (Figures 9A, B), in which Bi aims at conversion of CO_2RR to HCOOH product and the Pd targets FAOR to the highly reversible conversion of CO_2-to-HCOOH. This reversible Zn–CO_2 battery exhibits 52.64% FE_{HCOOH} (Figure 9C) and 45 h cycling durability. Despite the

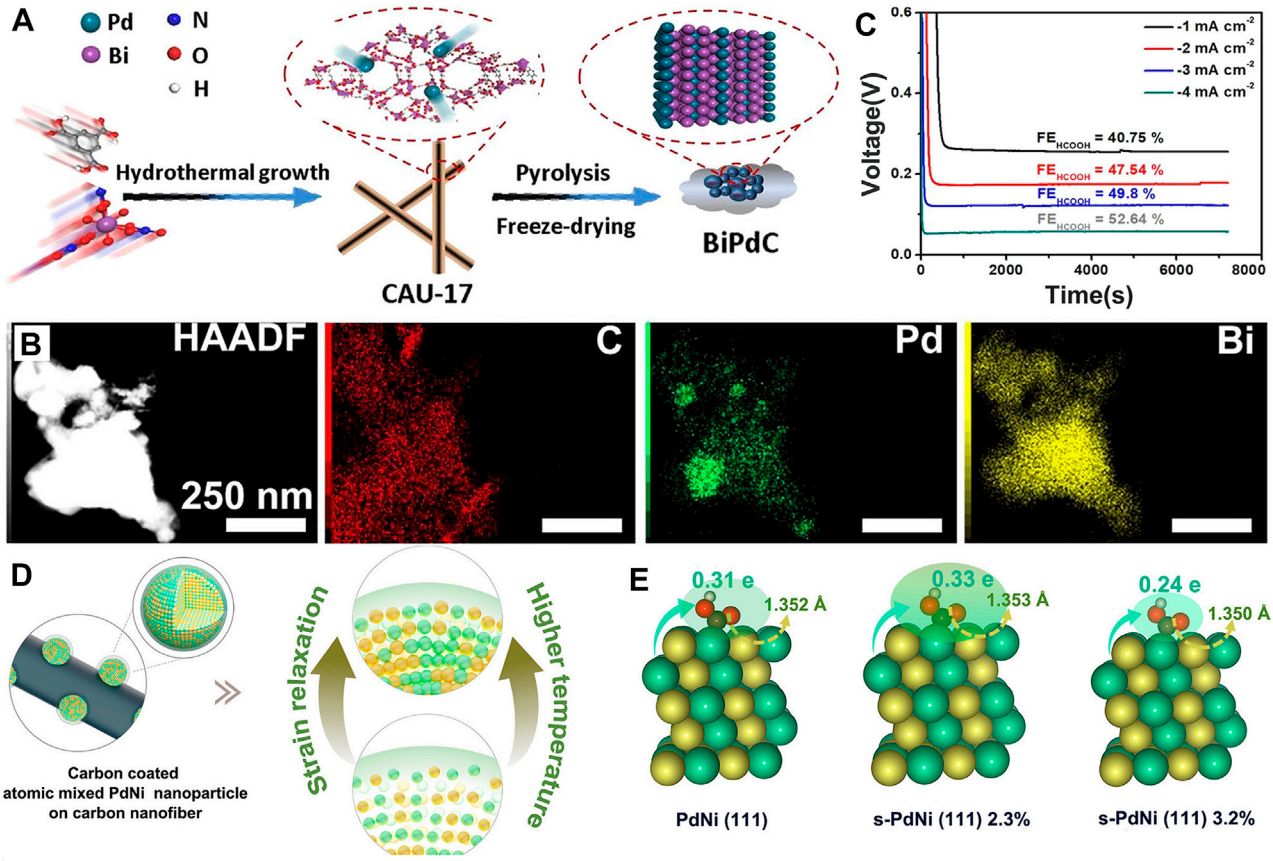

FIGURE 9
(A) Schematic illustration and **(B)** HAADF and DEX mapping of BiPdC. **(C)** Galvanostatic discharge curves with corresponding FE_{HCOOH}. Reproduced with permission (Gao S. et al., 2022). Copyright 2022, American Chemical Society. **(D)** Schematic illustration of s-PdNi. Green, yellow, brown, and red balls refer to Ni, Pd, C, and O atoms, respectively. **(E)** Bader charge analyses of the optimized adsorption structure for intermediate *COOH on s-PdNi-2.3% (111) surfaces. Reproduced with permission (Hao et al., 2022). Copyright 2022, American Chemical Society.

low FE_{HCOOH}, it is of great significance to construct a truly reversible Zn–CO_2 battery. In addition, the vital role of metal lattice revealed strains on CO_2RR and strained PdNi alloy (s-PdNi) (Hao et al., 2022) was confined into carbon shells, presenting optimized *COOH adsorption and *CO desorption on s-PdNi-2.3% (111) surfaces through Bader charge analysis (Figures 9D, E).

For metal-carbon catalysts, introducing heteroatoms with large electronegativity (such as B, P, and S.) is mainly to regulate the local electron density of the metal, thereby providing appropriate adsorption energy for CO_2RR (Maulana et al., 2021; Peng et al., 2022a; Ma et al., 2022). To achieve P doping, Fe–P nanocrystals were *in situ* implanted into a ZIF template and calcined at high temperatures to prepare Fe-P@NCPs (Liu et al., 2022d). During high-temperature pyrolysis, the ZIF-8 cage separates and encapsulates ferrocene, converts 2-methylimidazole into an N-C skeleton, and the evaporation of Zn ions simultaneously induces Fe reduction and phosphating, thus forming Fe–P nanocrystals with high interfacial charge transfer capability and catalytic performance. Its FE_{CO} can reach 95% at −0.55 V (vs. RHE). The Zn–CO_2 battery with Fe-P@NCPs operates at ultra-high stability, exceeding 500 cycles (7 days) without obvious voltage attenuation. It was reported that P-doping promotes OER/ORR (Yang J. et al., 2019); Yang R. et al. (2019) co-doped Ni with N and P on graphene, forming Ni/PNG nanomaterials, and designed a dual-mode Zn–CO_2/Zn–O_2 battery realizing CO_2RR/OER/ORR trifunctional catalysis. Ni-N on Ni/PNG mainly catalyzes CO_2RR (He et al., 2020; Leverett et al., 2022) and assists the OER and ORR, while PG mainly works on the OER/ORR and inhibits the HER. The operational routine of dual-model batteries is controlled by supplying gas, which enlightens the integrated multifunctional energy conversion-storage devices.

Metal-carbon composite catalysts combine the superior catalytic performance of metal and the excellent electrical conductivity of carbon frames, presenting significant superiority in product selectivity and showing great potential as bifunctional catalysts.

3.4 Single-atom catalyst (SAC)

Derived from metal–carbon composite catalysts, the SAC is particularly noticeable, and the isolated single-metal atom behaves as an active center without interaction with adjacent metal atoms (Xu et al., 2018; Shah et al., 2021; Shah et al., 2022). Relying on the high atom utilization and unique coordination environment (Liu

et al., 2020; Zhuang et al., 2020), the SAC shows great potential for excellent activity, selectivity, and stability (Sun et al., 2019) in CO_2RR and oxidation reactions. However, in actual conditions, the reduction of a catalyst's particle size leads to a sharp increase in surface energy, hardly maintaining the atomic level dispersion and driving metal atoms to gather, forming nanoparticles (Zhu et al., 2021b; Lin et al., 2021; Lin et al., 2022). Metal oxides, hydroxides, and carbon-based materials are accepted as substrates to separate metal atoms (Yang D. et al., 2020; Wang R. et al., 2021; Wan and Wang, 2021). Summarizing reports on SAC in Zn–CO_2 batteries show that most substrates are carbon-based materials and the SAC exists in metal–nitrogen–carbon (M-N-C) mode (Chen Z. et al., 2022; Yujie Shi and Lou, 2022).

MOF with unique structures is becoming an alternative to preparing SAC and M-N-C catalysts mostly derived from ZIF-8 and ZIF-67 precursors (Ding et al., 2022; Song et al., 2022), which take dimethylimidazole as the organic ligand presenting the dodecahedral structure and fix the Zn^{2+} and Co^{2+} as ligand metals, respectively (Yang H. et al., 2020; Song et al., 2020; Mo et al., 2022). The *in situ* metal substitution and high-temperature calcination strategy is adopted to allow control over the coordination environment of metal center sites together with altering the porosity and conductivity of the carbon skeleton (Han W. et al., 2022; Fu et al., 2022). The Fe_1NC/S_1-1000 (Wang T. et al., 2020) catalyst with Fe-N_3 sites balances the adsorption of *COOH and *CO, achieving a peak power density of 0.6 mW cm^{-2} and FE_{CO} as high as 96% at a potential of −0.5 V. Similarly, Zhang Y. et al. (2021) proposed the strategy of post-synthetic metal substitution. Zn-SAC was designed in advance to build a controllable coordination environment, and then Zn was replaced with Ni to generate Ni-SAC (Ni-N_x-C), increasing the FE_{CO} as high as 95.6%, and this Zn–CO_2 battery circulates 100 times under 2 mA cm^{-2}. Phthalocyanine (Pc) or porphyrin presents a similar plane symmetry structure as the M-N_4-C catalyst and is also accepted as a precursor for the SAC. (Liang Z. et al., 2021; Cruz-Navarro et al., 2021; Ji et al., 2021; Wang H. et al., 2022). CoPc was uniformly distributed in three-dimensional N-doped hollow carbon spheres (NHC) and activated under CO_2 atmosphere to prepare defected CoPc@DNHCS-T (Gong et al., 2022). Its high-density carbon defect with pyridine nitrogen establishes a double-electron absorption effect that regulates the electronic structure of the Co atom, accelerating CO_2 activation and *COOH formation. As a result, the Zn–CO_2 battery obtained a maximum power density of 1.02 mW cm^{-2} and circulated for 44 cycles (~44 h) at 1 mA cm^{-2}. Its FE_{CO} was up to 94%.

Importantly, the number and coordination mode of N atoms in the SAC induce a local electron density change around the central metal atom, regulating the adsorption of reaction intermediates and catalytic activity. (Yan et al., 2018; Lu et al., 2020) Liu et al. (2022c) anchored an Fe single atom on a B/N co-doped carbon matrix to form the Fe-SA/BNC catalyst that aroused significant electron transfer of *COOH and reduced the energy barrier of *CO on FeN_3B sites in the desorption process (Figures 10A–C) compared with Fe-N_4 sites based on DFT simulations. The Zn–CO_2 battery assembled with Fe-SA/BNC obtained a high power density of 1.18 mW cm^{-2}. Affected by the planar structure of M-N_4, the coupling rate of proton–electron is slow in the CO_2RR, and it requires higher reaction-free energy. Thus, the unique Fe-N_5 sites with axial N coordination on defective porous carbon nanofibers (Fe-N_5/DPCF) (Li Z. et al., 2022) (Figures 10D, E) were prepared via the facile dicyandiamide-assisted annealing method. Here, Fe is axially coordinated with N atoms on adjacent N-doped carbon layers, and the unstable pyrrole nitrogen and pyridine nitrogen sites on the CF substrate are removed, which leave intrinsic defects (Figures 10F, G). The theoretical calculations revealed that Fe-N_5/DPCF plays a key role in boosting CO_2RR (Figure 10H). Unlike plane Zn-N_4 sites, highly active asymmetric Zn-N_{3+1} in Zn/NC NSs (Chen J. et al., 2022) (Figures 11A, B) was developed. The Zn atom center is coordinated with four N atoms at the edges of two adjacent graphite atoms to form a twisted Zn-N_{3+1} structure, which promotes H_2O dissociation, accelerates proton–electron coupling, and reduces the energy barrier of *COOH (Figure 11C). Thus, its FE_{CO} is increased to 95% with a maximum battery power density of 1.8 mW cm^{-2}. It performs stable runs for 100 cycles (~26 h) under 1.5 mA cm^{-2}.

As reported, the catalytic effect of N-C configurations in CO_2RR is different and ranked as pyridine nitrogen > graphite nitrogen > pyrrole nitrogen, and these configurations can be altered via regulating the metal complex precursor or pyrolysis conditions (Hu et al., 2021b). For richer pyridine nitrogen, nickel 8-hydroxyquinoline complex (Ni-HQ) as a precursor mixed with melamine is pyrolyzed into Ni-doped graphite nanocarbon (Ni-Nx-2D/NPC) (Zeng et al., 2021) (Figures 11D–F). Pyridine nitrogen improves CO_2 capture capacity, and Ni-N sites inhibit the HER, cooperatively promoting CO_2RR selectivity under wide potential and high current density. The FE_{CO} is continuously raised above 90% and even nearly approaches 100% (Figure 7N).

SACs with fully exposed sites and a unique coordination environment improve the selective adsorption of specific functional groups, activation of reactants, and regulation of catalytic reactions (Chen et al., 2018; Liu L. et al., 2022). They show great potential in the field of catalysis and would play a vital role in future Zn–CO_2 batteries.

4 Summary and outlook

For aqueous Zn-CO_2 secondary batteries, the CO_2RR process captures and transfers CO_2 into value-added products such as $COOH^-$/CH_4 while also generating green electricity. In addition to the opposite charge process, it rarely produces CO_2 again, consuming CO_2 as a whole, which is in line with the CCUS strategy with broad prospects. However, problems such as unstable reaction kinetics, limited electrolyte environment, and poor product selectivity impede the application of Zn–CO_2 batteries. Here, catalyst design plays a decisive role in obtaining high-performance Zn–CO_2 batteries.

In this review, the structure and the involved reaction mechanism of CO_2RR/FAOR/OER in the aqueous Zn–CO_2 battery have been discussed; the preparation method and the strategy to develop cathode catalysts have also been summarized, especially for SAC materials. In summary, carbon-based catalysts contain excellent conductivity, large specific surface area, and abundant resources, showing obvious advantages in superior stability (Paul et al., 2019; Yuan and Lu, 2019; Hu et al., 2021a; Wang J. et al., 2021), but they are far from meeting application demands. Metal-based materials are considered effective catalysts with special geometry (Back et al., 2018), lattice defects, dispersion, and electron distribution (Jiang et al., 2018; Wang Y. et al., 2020).

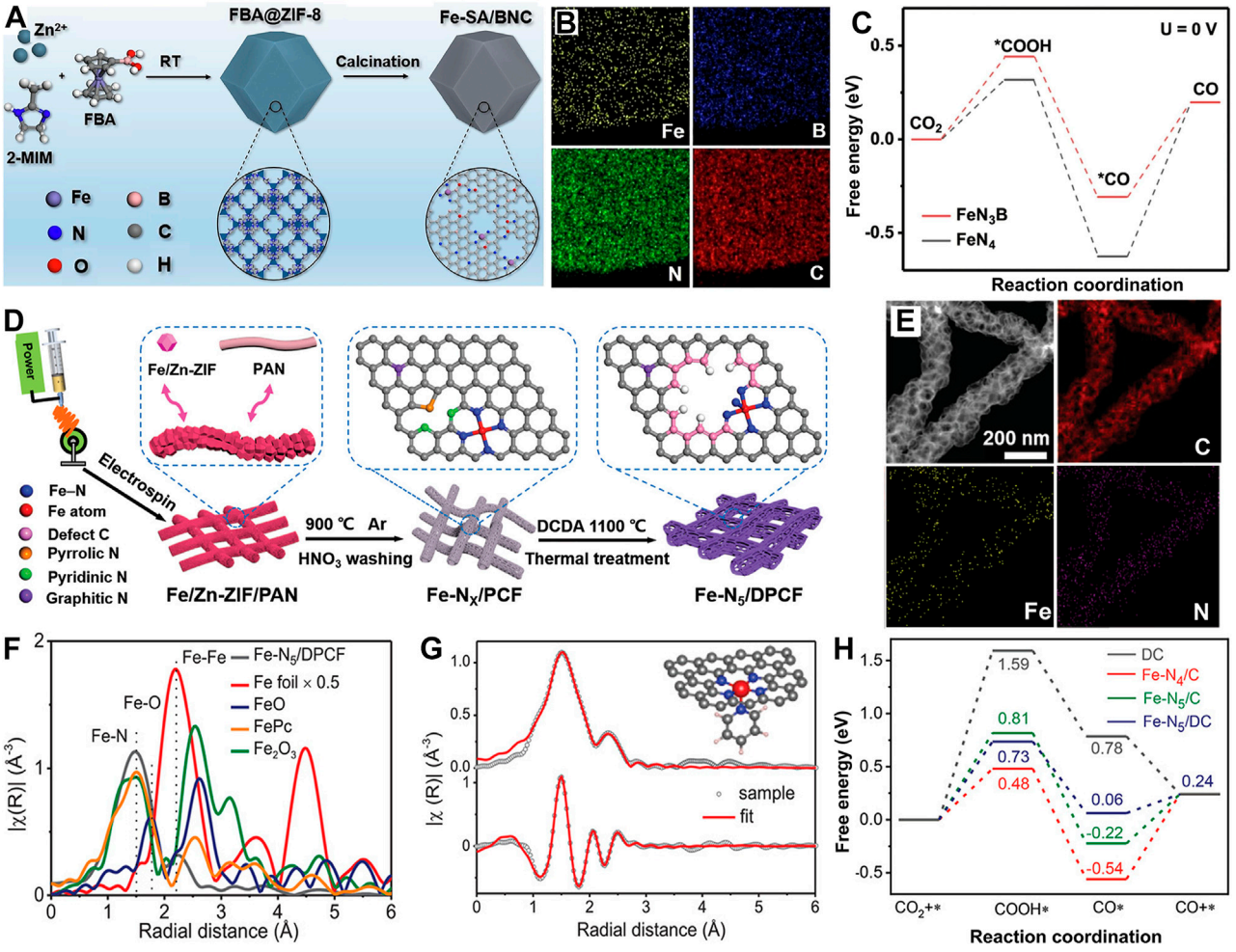

FIGURE 10
(A) Schematic illustrations and **(B)** EDX mapping of Fe-SA/BNC. **(C)** Mechanism research of CO_2RR pathway on FeN_4 and FeN_3B. Reproduced with permission (Liu et al., 2022c). Copyright 2022, Elsevier. **(D)** Schematic illustrations of Fe-N_5/DPCF. **(E)** HAADF-STEM image and STEM-EDS elemental maps of Fe-N_5/DPCF. **(F)** Fourier transformed curves of Fe K-edge EXAFS spectra. **(G)** Fe K-edge EXAFS fitting result of Fe-N_5/DPCF, inset shows the proposed 3D Fe-N_5 structure. **(H)** Free-energy profiles of reaction intermediates in CO_2RR. Reproduced with permission (Li Z. et al., 2022). Copyright 2022, Wiley.

Alloys with low cost and toxicity are becoming their alternatives. Furthermore, metal–carbon composite catalysts are being developed to pursue the integration of excellent stability and catalytic activity (Ding et al., 2019; Wang H. F. et al., 2020; Wang and Astruc, 2020). To tap the potential of metal–carbon composite catalysts to the fullest extent possible, the following strategy is adopted: 1) isolating single-metal sites for fully exposed active sites; (Jiao et al., 2020); 2) steady and high-conductivity carbon support (Sun et al., 2021). Thus, single-atom catalysts (SACs) are initiated and applied in Zn–CO_2 batteries.

Cathode catalysts are expected to achieve high value-added and high yields of products. More attention should be paid to product selectivity for multi-carbon chemicals and their bi-functional properties in both reduction and oxidation reactions for Zn–CO_2 systems. Catalyst design and structure regulation/optimization at the atomic level are recognized as feasible solutions. Herein, we propose the following strategies (Figure 12):

1) Reasonably design the catalyst structure.

The construction of catalysts with a large specific surface area and feasible pore structure is conducive to the accessibility of active sites where the rich mesoporous structure is profitable for the transport and storage of reactants and intermediates. Furthermore, this structure maintains the catalyst's stability, thus preventing the collapse of the internal structure during battery operation.

2) Promote catalyst conductivity.

Conductivity is a vital factor for both electrochemical mass transfer and proton–electron coupling rates. It is possible to introduce carbon frames, lattice defects, and heterostructures.

3) Develop catalytic sites with intrinsic activity.

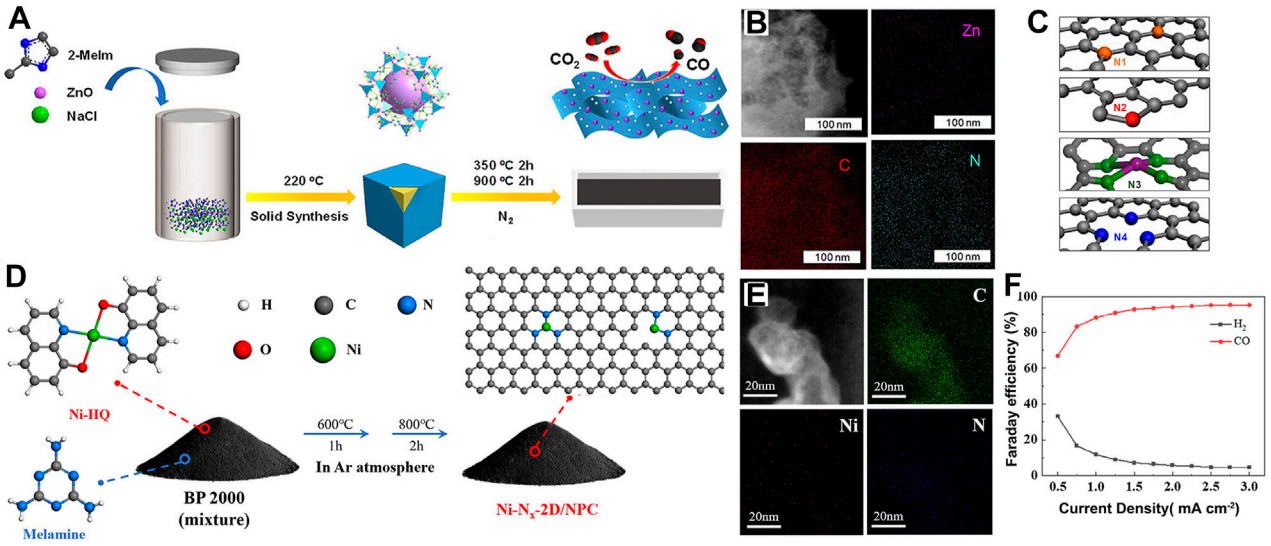

FIGURE 11
(A) Schematic illustrations and **(B)** TEM and EDS mapping of Zn/NC NSs. **(C)** Diagrams of different types of N atoms in Zn/NC NSs-T. Reproduced with permission (Chen J. et al., 2022). Copyright 2022, Wiley. **(D)** Schematic illustrations and **(E)** HAADF and corresponding EDX mappings of Ni-N_x-2D/NPC. **(F)** FE curves of Ni-N_x-2D/NPC cathode cells. Reproduced with permission (Zeng et al., 2021). Copyright 2021, Wiley.

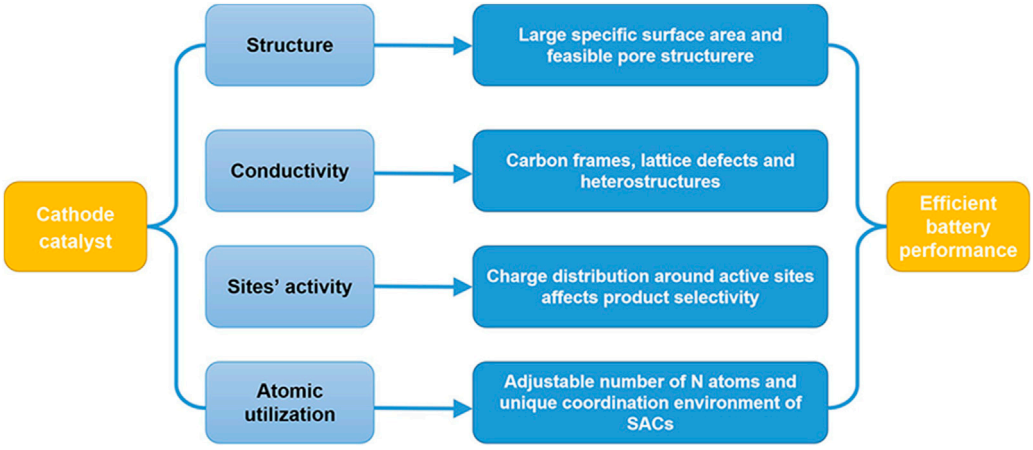

FIGURE 12
Cathode catalyst design strategy for Zn–CO_2 systems.

Charge distributions around active atoms influence the adsorption capacity of interaction intermediates/products, resulting in product selectivity and efficiency. Tackling competitive adsorption between *H, *COOH, *CO, and *OCHO in the catalytic process is crucial to the targeted products.

4) Improve atom utilization and create a unique coordination environment for SACs.

The adjustable number and coordination mode of N atoms in the SAC present an asymmetric or twisted structure that disrupts uniform charge distribution, resulting in highly desired catalytic properties.

In addition, aiming at the problems of self-corrosion, dendrite, and even hydrogen evolution in the anode of Zn–CO_2 batteries, the reported SEI interface engineering strategy can effectively stabilize the charge–discharge reaction process of the anode, inhibit the formation of zinc dendrites, and reduce the HER process. The excessive reaction of zinc can also be slowed by adding additives to the zinc electrode or by using a polymer film to prevent direct contact between zinc and the water-based electrolyte. Furthermore, the presence of Zn can be altered. For example, Zn is deposited into the collectors as graphene or stainless steel mesh, alternatively, or combined with other metals such as Cu, forming alloys to enhance the anode's stability.

At present, most Zn–CO_2 battery devices are assembled in H-type electrolytic cells. Their open-circuit voltage is 1–1.5 V, the charge voltage is generally below 2.6 V, and the cycle number is limited, which is far from commercial requirements. This limited performance is caused by its special bipolar membrane in a two-sided electrolyte environment and huge mass/volume of the device. In order to further increase the current and voltage of the device, the overall volume of the device should be compressed as much as possible, and the asymmetric structure of the membrane electrode and gas diffusion electrode should be modified to reduce the contact resistance of each component. On one hand, the hydrophilic and hydrophobic properties on both sides of the membrane electrode can be used to extend the service life of the anode and accelerate the charge–discharge reaction at the three-phase boundary. In addition, the gas diffusion layer can be increased to improve the amount of gas dissolution and accelerate the process of proton–electron coupling.

On the aforementioned bases, advanced *in situ* characterization techniques such as Raman, XPS, XRD, DEMS, and EXAFS and related theoretical calculations are suggested to deeply explore further the electrochemistry mechanism/process in Zn–CO_2 batteries, to guide the catalyst design, and to further increase the development toward high-performance batteries, multi-function devices, and/or multi-mode units with continuous expanding application potential.

Author contributions

WG and YW wrote the manuscript, and QY, ED, and LS revised the manuscript. PL, WS, and KQ designed and organized figures. XL conceived the idea, designed the structure of the review, revised the draft of the manuscript, supervised the work, and provided funding support. LG revised the draft of the manuscript and supervised the work. All authors contributed to the article and approved the submitted version.

Funding

This work was supposed by the National Natural Science Foundation of China (No. 52103307), the Fundamental Research Program of Shanxi Province (Nos. 20210302124015 and 20210302124003), and the General Program of Shanxi Province (No. 202203021211150).

Conflict of interest

Authors XL was employed by Shanxi Zhongke Huaneng Technology Co., Ltd.

The remaining authors declare that the research was conducted in the absence of any commercial or financial relationships that could be construed as a potential conflict of interest.

Publisher's note

All claims expressed in this article are solely those of the authors and do not necessarily represent those of their affiliated organizations, or those of the publisher, the editors, and the reviewers. Any product that may be evaluated in this article, or claim that may be made by its manufacturer, is not guaranteed or endorsed by the publisher.

References

Ahmadiparidari, A., Warburton, R. E., Majidi, L., Asadi, M., Chamaani, A., Jokisaari, J. R., et al. (2019). A long-cycle-life lithium-CO_2 battery with carbon neutrality. *Adv. Mater* 31 (40), e1902518. doi:10.1002/adma.201902518

Ansari, M. Z., Ansari, S. A., and Kim, S.-H. (2022). Fundamentals and recent progress of Sn-based electrode materials for supercapacitors: A comprehensive review. *J. Energy Storage* 53, 105187. doi:10.1016/j.est.2022.105187

Asadi, M., Sayahpour, B., Abbasi, P., Ngo, A. T., Karis, K., Jokisaari, J. R., et al. (2018). A lithium-oxygen battery with a long cycle life in an air-like atmosphere. *Nature* 555 (7697), 502–506. doi:10.1038/nature25984

Aslam, M. K., Wang, H., Chen, S., Li, Q., and Duan, J. (2023). Progress and perspectives of metal (Li, Na, Al, Zn and K)–CO2 batteries. *Mater. Today Energy* 31, 101196. doi:10.1016/j.mtener.2022.101196

Asokan, A., Lim, C., Kim, J., Kwon, O., Lee, H., Joo, S., et al. (2020). Carbon nanofibers encapsulated nickel-molybdenum nanoparticles as hydrogen evolution catalysts for aqueous Zn-CO_2 system. *ChemNanoMat* 6 (6), 937–946. doi:10.1002/cnma.202000099

Back, S., Yeom, M. S., and Jung, Y. (2018). Understanding the effects of Au morphology on CO_2 electrocatalysis. *J. Phys. Chem. C* 122 (8), 4274–4280. doi:10.1021/acs.jpcc.7b10439

Belotcerkovtceva, D., Maciel, R. P., Berggren, E., Maddu, R., Sarkar, T., Kvashnin, Y. O., et al. (2022). Insights and implications of intricate surface charge transfer and sp^3-defects in graphene/metal oxide interfaces. *ACS Appl. Mater Interfaces* 14 (31), 36209–36216. doi:10.1021/acsami.2c06626

Cai, F., Hu, Z., and Chou, S. L. (2018). Progress and future perspectives on Li(Na)-CO_2 batteries. *Adv. Sustain. Syst.* 2, 1800060–1800069. doi:10.1002/adsu.201800060

Calderón-Cárdenas, A., Hartl, F. W., Gallas, J. A. C., and Varela, H. (2021). Modeling the triple-path electro-oxidation of formic acid on platinum: Cyclic voltammetry and oscillations. *Catal. Today* 359, 90–98. doi:10.1016/j.cattod.2019.04.054

Cao, L., Fang, S., Xu, B., Zhang, B., Wang, C., Xiao, Z., et al. (2022). Enabling reversible reaction by uniform distribution of heterogeneous intermediates on defect-rich SnSSe/C layered heterostructure for ultralong-cycling sodium storage. *Small* 18 (26), e2202134. doi:10.1002/smll.202202134

Chang, Z., Xu, J., and Zhang, X. (2017). Recent progress in electrocatalyst for Li-O_2 batteries. *Adv. Energy Mater.* 7 (23), 1700875. doi:10.1002/aenm.201700875

Chen, B., Wang, D., Zhang, B., Zhong, X., Liu, Y., Sheng, J., et al. (2021a). Engineering the active sites of graphene catalyst: From CO_2 activation to activate Li-CO_2 batteries. *ACS Nano* 15 (6), 9841–9850. doi:10.1021/acsnano.1c00756

Chen, J., Li, Z., Wang, X., Sang, X., Zheng, S., Liu, S., et al. (2022a). Promoting CO_2 electroreduction kinetics on atomically dispersed monovalent Zn^1 sites by rationally engineering proton-feeding centers. Angew. Chem. Int. Ed. Engl. *(2022a)* 61 (7), e202111683. doi:10.1002/anie.202111683

Chen, S., Li, X., Kao, C. W., Luo, T., Chen, K., Fu, J., et al. (2022b). Unveiling the proton-feeding effect in sulfur-doped Fe-N-C single-atom catalyst for enhanced CO_2 electroreduction. Angew. Chem. Int. Ed. Engl. *(2022b)* 61 (32), e202206233. doi:10.1002/anie.202206233

Chen, S., Liu, J., Zhang, Q., Teng, F., and McLellan, B. C. (2022c). A critical review on deployment planning and risk analysis of carbon capture, utilization, and storage (CCUS) toward carbon neutrality. *Renew. Sustain. Energy Rev.* 167, 112537. doi:10.1016/j.rser.2022.112537

Chen, Y., Ji, S., Chen, C., Peng, Q., Wang, D., and Li, Y. (2018). Single-atom catalysts: Synthetic strategies and electrochemical applications. *Joule* 2 (7), 1242–1264. doi:10.1016/j.joule.2018.06.019

Chen, Y., Mei, Y., Li, M., Dang, C., Huang, L., Wu, W., et al. (2021b). Highly selective CO_2 conversion to methane or syngas tuned by CNTs@non-noble-metal cathodes in Zn-CO_2 flow batteries. *Green Chem.* 23 (20), 8138–8146. doi:10.1039/d1gc02496e

Chen, Z., Liu, J., Koh, M. J., and Loh, K. P. (2022d). Single-atom catalysis: From simple reactions to the synthesis of complex molecules. *Adv. Mater* 34 (25), e2103882. doi:10.1002/adma.202103882

Chhetri, K., Kim, T., Acharya, D., Muthurasu, A., Dahal, B., Bhattarai, R. M., et al. (2022). Hollow carbon nanofibers with inside-outside decoration of Bi-metallic MOF derived Ni-Fe phosphides as electrode materials for asymmetric supercapacitors. *Chem. Eng. J.* 450, 138363. doi:10.1016/j.cej.2022.138363

Chu, S., Cui, Y., and Liu, N. (2016). The path towards sustainable energy. *Nat. Mater* 16 (1), 16–22. doi:10.1038/nmat4834

Cruz-Navarro, J. A., Hernández-García, F., Mendoza-Huizar, L. H., Salazar-Pereda, V., Cobos-Murcia, J. . Á., Colorado-Peralta, R., et al. (2021). Recent advances in the use of transition-metal porphyrin and phthalocyanine complexes as electro-catalyst materials on modified electrodes for electroanalytical sensing applications. *Solids* 2 (2), 212–231. doi:10.3390/solids2020014

de Oliveira Maciel, A., Christakopoulos, P., Rova, U., and Antonopoulou, I. (2022). Carbonic anhydrase to boost CO_2 sequestration: Improving carbon capture utilization and storage (CCUS). *Chemosphere* 299, 134419. doi:10.1016/j.chemosphere.2022.134419

Deng, P., Yang, F., Wang, Z., Chen, S., Zhou, Y., Zaman, S., et al. (2020). Metal-organic framework-derived carbon nanorods encapsulating bismuth oxides for rapid and selective CO_2 electroreduction to formate. *Angew. Chem. Int. Ed. Engl.* 59 (27), 10807–10813. doi:10.1002/anie.202000657

Ding, J., Xue, H., Xiao, R., Xu, Y., Song, L., Gong, H., et al. (2022). Atomically dispersed Fe-nx species within a porous carbon framework: An efficient catalyst for Li-CO_2 batteries. *Nanoscale* 14 (12), 4511–4518. doi:10.1039/d1nr08354f

Ding, M., Flaig, R. W., Jiang, H. L., and Yaghi, O. M. (2019). Carbon capture and conversion using metal-organic frameworks and MOF-based materials. *Chem. Soc. Rev.* 48 (10), 2783–2828. doi:10.1039/c8cs00829a

Dong, Y., Ghuman, K. K., Popescu, R., Duchesne, P. N., Zhou, W., Loh, J. Y. Y., et al. (2018). Tailoring surface frustrated lewis pairs of In_2O_{3-x} $(OH)_y$ for gas-phase heterogeneous photocatalytic reduction of CO_2 by isomorphous substitution of In^{3+} with Bi^{3+}. *Adv. Sci. (Weinh)* 5 (6), 1700732. doi:10.1002/advs.201700732

El Sawy, E. N., and Pickup, P. G. (2016). Formic acid oxidation at Ru@Pt core-shell nanoparticles. *Electrocatalysis* 7 (6), 477–485. doi:10.1007/s12678-016-0328-8

Eskezia Ayalew, M. (2021). The role of nanotechnology for energy storage, conservation and post combustion CO_2 capture in industry: A review. *Int. J. Mater. Sci. Appl.* 10 (3), 55. doi:10.11648/j.ijmsa.20211003.12

Fan, L., Xu, J., and Hong, Y. (2022). Defects in graphene-based heterostructures: Topological and geometrical effects. *RSC Adv.* 12 (11), 6772–6782. doi:10.1039/d1ra08884j

Feng, Z.-y., Peng, W.-j., Wang, Z.-x., Guo, H.-j., Li, X.-h., Yan, G.-c., et al. (2021). Review of silicon-based alloys for lithium-ion battery anodes. *Int. J. Minerals, Metallurgy Mater.* 28 (10), 1549–1564. doi:10.1007/s12613-021-2335-x

Fu, L., Chen, H., Wang, K., and Wang, X. (2022). Oxygen-vacancy generation in $MgFe_2O_4$ by high temperature calcination and its improved photocatalytic activity for CO_2 reduction. *J. Alloys Compd.* 891, 161925. doi:10.1016/j.jallcom.2021.161925

Gao, S., Chen, S., Liu, Q., Zhang, S., Qi, G., Luo, J., et al. (2022a). Bifunctional BiPd alloy particles anchored on carbon matrix for reversible Zn-CO_2 battery. *ACS Appl. Nano Mater.* 5 (9), 12387–12394. doi:10.1021/acsanm.2c02917

Gao, S., Jin, M., Sun, J., Liu, X., Zhang, S., Li, H., et al. (2021a). Coralloid Au enables high-performance Zn-CO_2 battery and self-driven CO production. *J. Mater. Chem. A* 9 (37), 21024–21031. doi:10.1039/d1ta04360a

Gao, S., Liu, Y., Xie, Z., Qiu, Y., Zhuo, L., Qin, Y., et al. (2021b). Metal-free bifunctional ordered mesoporous carbon for reversible Zn-CO_2 batteries. *Small Methods* 5 (4), 2001039. doi:10.1002/smtd.202001039

Gao, Y., and Zhao, L. (2022). Review on recent advances in nanostructured transition-metal-sulfide-based electrode materials for cathode materials of asymmetric supercapacitors. *Chem. Eng. J.* 430, 132745. doi:10.1016/j.cej.2021.132745

Gao, Y., Zhao, Y., Liu, H., Shao, M., Chen, Z., Ma, T., et al. (2022b). N, P-doped carbon supported ruthenium doped Rhenium phosphide with porous nanostructure for hydrogen evolution reaction using sustainable energies. *J. Colloid Interface Sci.* 606, 1874–1881. doi:10.1016/j.jcis.2021.08.077

Ghausi, M. A., Xie, J., Li, Q., Wang, X., Yang, R., Wu, M., et al. (2018). CO_2 overall splitting by a bifunctional metal-free electrocatalyst. *Angew. Chem. Int. Ed. Engl.* 57 (40), 13135–13139. doi:10.1002/anie.201807571

Gong, Q., Ding, P., Xu, M., Zhu, X., Wang, M., Deng, J., et al. (2019). Structural defects on converted bismuth oxide nanotubes enable highly active electrocatalysis of carbon dioxide reduction. *Nat. Commun.* 10 (1), 2807. doi:10.1038/s41467-019-10819-4

Gong, S., Wang, W., Zhang, C., Zhu, M., Lu, R., Ye, J., et al. (2022). Tuning the metal electronic structure of anchored cobalt phthalocyanine via dual-regulator for efficient CO_2 electroreduction and Zn-CO_2 batteries. *Adv. Funct. Mater.* 32, 2110649. doi:10.1002/adfm.202110649

Guo, H., Wang, X., Wang, H., Cui, W., Li, M., and Xie, W. (2022a). Double-exchange-induced effective increased CO_2 capture of CaO by doping bimetallic oxides with variable valence state. *Chem. Eng. J.* 433, 134490. doi:10.1016/j.cej.2021.134490

Guo, Y., Zhang, R., Zhang, S., and Zhi, C. (2022b). Recent advances in Zn-CO_2 batteries for the co-production of electricity and carbonaceous fuels. *Nano Mater. Sci.* doi:10.1016/j.nanoms.2022.09.004

Han, L., Peng, X., Wang, H. T., Ou, P., Mi, Y., Pao, C. W., et al. (2022a). Chemically coupling SnO_2 quantum dots and MXene for efficient CO_2 electroreduction to formate and Zn-CO_2 battery. *Proc. Natl. Acad. Sci. U. S. A.* 119 (42), e2207326119. doi:10.1073/pnas.2207326119

Han, N., Wang, Y., Yang, H., Deng, J., Wu, J., Li, Y., et al. (2018). Ultrathin bismuth nanosheets from *in situ* topotactic transformation for selective electrocatalytic CO_2 reduction to formate. *Nat. Commun.* 9 (1), 1320. doi:10.1038/s41467-018-03712-z

Han, W., Xiong, L., Wang, M., Seo, W., Liu, Y., Taj Ud Din, S., et al. (2022b). Interface engineering via *in-situ* electrochemical induced ZnSe for a stabilized zinc metal anode. *Chem. Eng. J.* 442, 136247. doi:10.1016/j.cej.2022.136247

Hao, J., Li, X., Zeng, X., Li, D., Mao, J., and Guo, Z. (2020). Deeply understanding the Zn anode behaviour and corresponding improvement strategies in different aqueous Zn-based batteries. *Energy and Environ. Sci.* 13 (11), 3917–3949. doi:10.1039/d0ee02162h

Hao, J., Yuan, L., Ye, C., Chao, D., Davey, K., Guo, Z., et al. (2021). Boosting zinc electrode reversibility in aqueous electrolytes by using low-cost antisolvents. *Angew. Chem. Int. Ed. Engl.* 60 (13), 7366–7375. doi:10.1002/anie.202016531

Hao, J., Zhuang, Z., Hao, J., Cao, K., Hu, Y., Wu, W., et al. (2022). Strain relaxation in metal alloy catalysts steers the product selectivity of electrocatalytic CO_2 reduction. *ACS Nano* 16 (2), 3251–3263. doi:10.1021/acsnano.1c11145

He, Y., Li, Y., Zhang, J., Wang, S., Huang, D., Yang, G., et al. (2020). Low-temperature strategy toward Ni-NC@Ni core-shell nanostructure with Single-Ni sites for efficient CO_2 electroreduction. *Nano Energy* 77, 105010. doi:10.1016/j.nanoen.2020.105010

Hu, A., Shu, C., Xu, C., Liang, R., Li, J., Zheng, R., et al. (2019). Design strategies toward catalytic materials and cathode structures for emerging Li-CO_2 batteries. *J. Mater. Chem. A* 7 (38), 21605–21633. doi:10.1039/c9ta06506g

Hu, C., Dai, Q., and Dai, L. (2021a). Multifunctional carbon-based metal-free catalysts for advanced energy conversion and storage. *Cell Rep. Phys. Sci.* 2 (2), 100328. doi:10.1016/j.xcrp.2021.100328

Hu, C., Paul, R., Dai, Q., and Dai, L. (2021b). Carbon-based metal-free electrocatalysts: From oxygen reduction to multifunctional electrocatalysis. *Chem. Soc. Rev.* 50 (21), 11785–11843. doi:10.1039/d1cs00219h

Hu, H., Wang, J., Cui, B., Zheng, X., Lin, J., Deng, Y., et al. (2021c). Atomically dispersed selenium sites on nitrogen-doped carbon for efficient electrocatalytic oxygen reduction. *Angew. Chem. Int. Ed. Engl.* 61, e202114441. doi:10.1002/anie.202114441

Huang, C., Ji, Q., Zhang, H., Wang, Y., Wang, S., Liu, X., et al. (2022). Ru-incorporated Co_3O_4 nanoparticles from self-sacrificial ZIF-67 template as efficient bifunctional electrocatalysts for rechargeable metal-air battery. *J. Colloid Interface Sci.* 606, 654–665. doi:10.1016/j.jcis.2021.08.046

Huang, Y., Wang, Y., Tang, C., Wang, J., Zhang, Q., Wang, Y., et al. (2019). Atomic modulation and structure design of carbons for bifunctional electrocatalysis in metal-air batteries. *Adv. Mater* 31 (13), e1803800. doi:10.1002/adma.201803800

Ji, W., Wang, T.-X., Ding, X., Lei, S., and Han, B.-H. (2021). Porphyrin- and phthalocyanine-based porous organic polymers: From synthesis to application. *Coord. Chem. Rev.* 439, 213875. doi:10.1016/j.ccr.2021.213875

Jiang, B., Zhang, X. G., Jiang, K., Wu, D. Y., and Cai, W. B. (2018). Boosting formate production in electrocatalytic CO_2 reduction over wide potential window on Pd surfaces. *J. Am. Chem. Soc.* 140 (8), 2880–2889. doi:10.1021/jacs.7b12506

Jiang, K., Ashworth, P., Zhang, S., and Hu, G. (2022). Print media representations of carbon capture utilization and storage (CCUS) technology in China. *Renew. Sustain. Energy Rev.* 155, 111938. doi:10.1016/j.rser.2021.111938

Jiao, L., Zhang, R., Wan, G., Yang, W., Wan, X., Zhou, H., et al. (2020). Nanocasting SiO_2 into metal-organic frameworks imparts dual protection to high-loading Fe single-atom electrocatalysts. *Nat. Commun.* 11 (1), 2831. doi:10.1038/s41467-020-16715-6

Jiao, L., Zhu, J., Zhang, Y., Yang, W., Zhou, S., Li, A., et al. (2021). Non-bonding interaction of neighboring Fe and Ni single-atom pairs on MOF-derived N-doped carbon for enhanced CO_2 electroreduction. *J. Am. Chem. Soc.* 143 (46), 19417–19424. doi:10.1021/jacs.1c08050

Kang, J., Rui, N., Rosales, R., Tian, Y., Senanayake, S. D., and Rodriguez, J. A. (2022a). Understanding the surface structure and catalytic activity of SnOx/Au(111) inverse catalysts for CO_2 and H_2 activation. *J. Phys. Chem. C* 126 (10), 4862–4870. doi:10.1021/acs.jpcc.2c00138

Kang, T., Nam, D., and Kim, J. (2022b). Activated palladium deposited on defect-rich carbon and cobalt oxide composite materials as bi-functional catalysts for stable rechargeable Zn-air battery. *Appl. Surf. Sci.* 582, 152442. doi:10.1016/j.apsusc.2022.152442

Khurram, A., He, M., and Gallant, B. M. (2018). Tailoring the discharge reaction in Li-CO_2 batteries through incorporation of CO_2 capture Chemistry. *Joule* 2 (12), 2649–2666. doi:10.1016/j.joule.2018.09.002

Kim, J., Yang, Y., Seong, A., Noh, H.-J., Kim, C., Joo, S., et al. (2020). Identifying the electrocatalytic active sites of a Ru-based catalyst with high Faraday efficiency in CO_2-

saturated media for an aqueous Zn-CO_2 system. *J. Mater. Chem. A* 8 (30), 14927–14934. doi:10.1039/d0ta03050c

Kong, F., Liu, X., Song, Y., Qian, Z., Li, J., Zhang, L., et al. (2022). Selectively coupling Ru single atoms to PtNi concavities for high performance methanol oxidation via d-band center regulation. *Angew. Chem. Int. Ed. Engl.* 61, e202207524. doi:10.1002/anie.202207524

Lankone, R. S., Wang, J., Ranville, J. F., and Fairbrother, D. H. (2017). Photodegradation of polymer-CNT nanocomposites: Effect of CNT loading and CNT release characteristics. *Environ. Sci. Nano* 4 (4), 967–982. doi:10.1039/c6en00669h

Lei, Z., Sathish, C. I., Liu, Y., Karokoti, A., Wang, J., Qiao, L., et al. (2022). Single metal atoms catalysts-Promising candidates for next generation energy storage and conversion devices. *EcoMat* 4 (3). doi:10.1002/eom2.12186

Leverett, J., Yuwono, J. A., Kumar, P., Tran-Phu, T., Qu, J., Cairney, J., et al. (2022). Impurity tolerance of unsaturated Ni-N-C active sites for practical electrochemical CO_2 reduction. *ACS Energy Lett.* 7 (3), 920–928. doi:10.1021/acsenergylett.1c02711

Li, D., Gao, Y., Xie, C., and Zheng, Z. (2022a). Au-coated carbon fabric as Janus current collector for dendrite-free flexible lithium metal anode and battery. *Appl. Phys. Rev.* 9 (1), 011424. doi:10.1063/5.0083830

Li, F., Chen, L., Knowles, G. P., MacFarlane, D. R., and Zhang, J. (2017). Hierarchical mesoporous SnO_2 nanosheets on carbon cloth: A robust and flexible electrocatalyst for CO_2 reduction with high efficiency and selectivity. *Angew. Chem. Int. Ed.* 129 (2), 505–509. doi:10.1002/anie.201608279

Li, Z., Jiang, J., Liu, X., Zhu, Z., Wang, J., He, Q., et al. (2022b). Coupling atomically dispersed Fe-N_5 sites with defective N-doped carbon boosts CO_2 electroreduction. *Small* 18 (38), e2203495. doi:10.1002/smll.202203495

Liang, M., Xia, T., Gao, H., Zhao, K., Cao, T., Deng, M., et al. (2021a). Modulating reaction pathways of formic acid oxidation for optimized electrocatalytic performance of PtAu/CoNC. *Nano Res.* 15 (2), 1221–1229. doi:10.1007/s12274-021-3629-z

Liang, Z., Wang, H. Y., Zheng, H., Zhang, W., and Cao, R. (2021b). Porphyrin-based frameworks for oxygen electrocatalysis and catalytic reduction of carbon dioxide. *Chem. Soc. Rev.* 50 (4), 2540–2581. doi:10.1039/d0cs01482f

Lichchhavi, K. A., and Shirage, P. M. (2022). A review on synergy of transition metal oxide nanostructured materials: Effective and coherent choice for supercapacitor electrodes. *J. Energy Storage* 22, 55. doi:10.1016/j.est.2022.105692

Lin, J., Ding, J., Wang, H., Yang, X., Zheng, X., Huang, Z., et al. (2022). Boosting energy efficiency and stability of Li-CO_2 batteries via synergy between Ru atom clusters and single-atom Ru-N_4 sites in the electrocatalyst cathode. *Adv. Mater* 34, e2200559. doi:10.1002/adma.202200559

Lin, L., Gerlak, C. A., Liu, C., Llorca, J., Yao, S., Rui, N., et al. (2021). Effect of Ni particle size on the production of renewable methane from CO_2 over Ni/CeO_2 catalyst. *J. Energy Chem.* 61, 602–611. doi:10.1016/j.jechem.2021.02.021

Ling, L. L., Jiao, L., Liu, X., Dong, Y., Yang, W., Zhang, H., et al. (2022). Potassium-assisted fabrication of intrinsic defects in porous carbons for electrocatalytic CO_2 reduction. *Adv. Mater* 34 (42), e2205933. doi:10.1002/adma.202205933

Liu, D., He, Q., Ding, S., and Song, L. (2020). Structural regulation and support coupling effect of single-atom catalysts for heterogeneous catalysis. *Adv. Energy Mater.* 10 (32), 2001482. doi:10.1002/aenm.202001482

Liu, K., Meng, X., Yan, L., Fan, M., Wu, Y., Li, C., et al. (2022a). Sn/SnO_x core-shell structure encapsulated in nitrogen-doped porous carbon frameworks for enhanced lithium storage. *J. Alloys Compd.* 896, 163009. doi:10.1016/j.jallcom.2021.163009

Liu, L., Li, M., Chen, F., and Huang, H. (2022b). Recent advances on single-atom catalysts for CO_2 reduction. *Small Struct.* 4 (3), 2200188. doi:10.1002/sstr.202200188

Liu, S., Jin, M., Sun, J., Qin, Y., Gao, S., Chen, Y., et al. (2022c). Coordination environment engineering to boost electrocatalytic CO_2 reduction performance by introducing boron into single-Fe-atomic catalyst. *Chem. Eng. J.* 437, 135294. doi:10.1016/j.cej.2022.135294

Liu, S., Wang, L., Yang, H., Gao, S., Liu, Y., Zhang, S., et al. (2022d). Nitrogen-doped carbon polyhedrons confined Fe-P nanocrystals as high-efficiency bifunctional catalysts for aqueous Zn-CO_2 batteries. *Small* 18, e2104965. doi:10.1002/smll.202104965

Lu, B., Liu, Q., and Chen, S. (2020). Electrocatalysis of single-atom sites: Impacts of atomic coordination. *ACS Catal.* 10 (14), 7584–7618. doi:10.1021/acscatal.0c01950

Lü, F., Qi, G., Liu, X., Zhang, C., Guo, R., Peng, X., et al. (2019). Selective electrolysis of CO_2 to CO on ultrathin In_2Se_3 nanosheets. *Electrochem. Commun.* 103, 127–132. doi:10.1016/j.elecom.2019.05.020

Ma, G., Ning, G., and Wei, Q. (2022). S-doped carbon materials: Synthesis, properties and applications. *Carbon* 195, 328–340. doi:10.1016/j.carbon.2022.03.043

Ma, W., Liu, X., Li, C., Yin, H., Xi, W., Liu, R., et al. (2018). Rechargeable Al-CO_2 batteries for reversible utilization of CO_2. *Adv. Mater* 30 (28), e1801152. doi:10.1002/adma.201801152

Maulana, A. L., Saputro, A. G., Prasetyo, Y., Mahyuddin, M. H., Iqbal, M., Yudistira, H. T., et al. (2021). Two-electron electrochemical reduction of CO_2 on B-doped Ni-N-C catalysts: A first-principles study. *J. Phys. Chem. C* 125 (35), 19247–19258. doi:10.1021/acs.jpcc.1c04986

Mo, Z., Tai, D., Zhang, H., and Shahab, A. (2022). A comprehensive review on the adsorption of heavy metals by zeolite imidazole framework (ZIF-8) based nanocomposite in water. *Chem. Eng. J.* 443, 136320. doi:10.1016/j.cej.2022.136320

Mu, X., Pan, H., He, P., and Zhou, H. (2020). Li-CO_2 and Na-CO_2 batteries: Toward greener and sustainable electrical energy storage. *Adv. Mater* 32 (27), e1903790. doi:10.1002/adma.201903790

Paul, R., Dai, Q., Hu, C., and Dai, L. (2019). Ten years of carbon-based metal-free electrocatalysts. *Carbon Energy* 1 (1), 19–31. doi:10.1002/cey2.5

Peng, M., Ci, S., Shao, P., Cai, P., and Wen, Z. (2019). Cu_3P/C nanocomposites for efficient electrocatalytic CO_2 reduction and Zn-CO_2 battery. *J. Nanosci. Nanotechnol.* 19 (6), 3232–3236. doi:10.1166/jnn.2019.16589

Peng, Y., Bai, Y., Liu, C., Cao, S., Kong, Q., and Pang, H. (2022a). Applications of metal–organic framework-derived N, P, S doped materials in electrochemical energy conversion and storage. *Coord. Chem. Rev.* 466, 214602. doi:10.1016/j.ccr.2022.214602

Peng, Y., Xu, J., Xu, J., Ma, J., Bai, Y., Cao, S., et al. (2022b). Metal-organic framework (MOF) composites as promising materials for energy storage applications. *Adv. Colloid Interface Sci.* 307, 102732. doi:10.1016/j.cis.2022.102732

Pfeiffer, O., Khurram, A., Olivetti, E. A., and Gallant, B. M. (2022). Life cycle assessment of CO_2 conversion and storage in metal-CO_2 electrochemical cells. *J. Industrial Ecol.* 26, 1306–1317. doi:10.1111/jiec.13266

Qiao, Y., Yi, J., Wu, S., Liu, Y., Yang, S., He, P., et al. (2017). Li-CO_2 electrochemistry: A new strategy for CO_2 fixation and energy storage. *Joule* 1 (2), 359–370. doi:10.1016/j.joule.2017.07.001

Raknual, D., Charoenphon, S., Reunchan, P., and Tubtimtae, A. (2021). Structural and electrochemical properties of undoped and In^{3+}-doped multi-phase zinc-antimony oxide for a high-performance pseudocapacitor. *Electrochimica Acta* 389, 138773. doi:10.1016/j.electacta.2021.138773

Sawant, S. V., Patwardhan, A. W., Joshi, J. B., and Dasgupta, K. (2022). Boron doped carbon nanotubes: Synthesis, characterization and emerging applications - a review. *Chem. Eng. J.* 427, 131616. doi:10.1016/j.cej.2021.131616

Selvakumaran, D., Pan, A., Liang, S., and Cao, G. (2019). A review on recent developments and challenges of cathode materials for rechargeable aqueous Zn-ion batteries. *J. Mater. Chem. A* 7 (31), 18209–18236. doi:10.1039/c9ta05053a

Shah, S. S. A., Najam, T., Bashir, M. S., Peng, L., Nazir, M. A., and Javed, M. S. (2022). Single-atom catalysts for next-generation rechargeable batteries and fuel cells. *Energy Storage Mater.* 45, 301–322. doi:10.1016/j.ensm.2021.11.049

Shah, S. S. A., Najam, T., Javed, M. S., Bashir, M. S., Nazir, M. A., Khan, N. A., et al. (2021). Recent advances in synthesis and applications of single-atom catalysts for rechargeable batteries. *Chem. Rec.* 22, e202100280. doi:10.1002/tcr.202100280

Shakeri, M., Khatami Shal, Z., and Van Der Voort, P. (2021). An overview of the challenges and progress of synthesis, characterization and applications of plugged SBA-15 materials for heterogeneous catalysis. *Mater. (Basel)* 14 (17), 5082. doi:10.3390/ma14175082

Shi, Q., Liu, Q., Zheng, Y., Dong, Y., Wang, L., Liu, H., et al. (2021). Controllable construction of bifunctional Co_xP@N,P-doped carbon electrocatalysts for rechargeable zinc-air batteries. *Energy and Environ. Mater.* 5 (2), 515–523. doi:10.1002/eem2.12208

Song, K., Feng, Y., Zhang, W., and Zheng, W. (2022). MOFs fertilized transition-metallic single-atom electrocatalysts for highly-efficient oxygen reduction: Spreading the synthesis strategies and advanced identification. *J. Energy Chem.* 67, 391–422. doi:10.1016/j.jechem.2021.10.011

Song, Z., Zhang, L., Doyle-Davis, K., Fu, X., Luo, J. L., and Sun, X. (2020). Recent advances in MOF-derived single atom catalysts for electrochemical applications. *Adv. Energy Mater.* 10 (38), 2001561. doi:10.1002/aenm.202001561

Spada, D., Bruni, P., Ferrari, S., Albini, B., Galinetto, P., Berbenni, V., et al. (2022). Self-Supported fibrous Sn/SnO_2@C nanocomposite as superior anode material for lithium-ion batteries. *Mater. (Basel)* 15 (3), 919. doi:10.3390/ma15030919

Su, J., Yuan, M., Han, L., Deng, H., Chang, J., Zhuang, Y., et al. (2022). Ultrathin metal organic framework nanosheets with rich defects for enhanced fluoride removal. *Chem. Eng. J.* 451, 138989. doi:10.1016/j.cej.2022.138989

Suen, N. T., Hung, S. F., Quan, Q., Zhang, N., Xu, Y. J., and Chen, H. M. (2017). Electrocatalysis for the oxygen evolution reaction: Recent development and future perspectives. *Chem. Soc. Rev.* 46 (2), 337–365. doi:10.1039/c6cs00328a

Sui, X., Zhang, L., Li, J., Doyle-Davis, K., Li, R., Wang, Z., et al. (2021). Advanced support materials and interactions for atomically dispersed noble-metal catalysts: From support effects to design strategies. *Adv. Energy Mater.* 12 (1), 2102556. doi:10.1002/aenm.202102556

Sun, T., Mitchell, S., Li, J., Lyu, P., Wu, X., Perez-Ramirez, J., et al. (2021). Design of local atomic environments in single-atom electrocatalysts for renewable energy conversions. *Adv. Mater* 33 (5), e2003075. doi:10.1002/adma.202003075

Sun, T., Xu, L., Wang, D., and Li, Y. (2019). Metal organic frameworks derived single atom catalysts for electrocatalytic energy conversion. *Nano Res.* 12 (9), 2067–2080. doi:10.1007/s12274-019-2345-4

Tan, Z., Zhang, J., Yang, Y., Sha, Y., Duan, R., Zhong, J., et al. (2022). BiO_{2-x} nanosheets with surface electron localizations for efficient electrocatalytic CO_2 reduction to formate. *CCS Chem.* 5, 133–144. doi:10.31635/ccschem.022.202202068

Teng, X., Lu, J., Niu, Y., Gong, S., Xu, M., Meyer, T. J., et al. (2022). Selective CO_2 reduction to formate on a Zn-based electrocatalyst promoted by tellurium. *Chem. Mater.* 34 (13), 6036–6047. doi:10.1021/acs.chemmater.2c01131

Teng, X., Niu, Y., Gong, S., Xu, M., Liu, X., Ji, L., et al. (2021)./ZnO@C hollow nanocubes for efficient electrochemical reduction of CO_2 to formate and rechargeable Zn-CO_2 batteries. *Mater. Chem. Front.* 5 (17), 6618–6627. doi:10.1039/d1qm00825k

Thakur, A. K., Kurtyka, K., Majumder, M., Yang, X., Ta, H. Q., Bachmatiuk, A., et al. (2022). Recent advances in boron- and nitrogen-doped carbon-based materials and their various applications. *Adv. Mater. Interfaces* 9 (11), 2101964. doi:10.1002/admi.202101964

Tian, J., Wang, R., Shen, M., Ma, X., Yao, H., Hua, Z., et al. (2021). Bi-Sn oxides for highly selective CO_2 electroreduction to formate in a wide potential window. *ChemSusChem* 14 (10), 2247–2254. doi:10.1002/cssc.202100543

Wan, L., and Wang, P. (2021). Recent progress on self-supported two-dimensional transition metal hydroxides nanosheets for electrochemical energy storage and conversion. *Int. J. Hydrogen Energy* 46 (12), 8356–8376. doi:10.1016/j.ijhydene.2020.12.061

Wang, C., Li, J., Zhou, Z., Pan, Y., Yu, Z., Pei, Z., et al. (2021a). Rechargeable zinc-air batteries with neutral electrolytes: Recent advances, challenges, and prospects. *EnergyChem* 3 (4), 100055. doi:10.1016/j.enchem.2021.100055

Wang, F., Li, Y., Xia, X., Cai, W., Chen, Q., and Chen, M. (2021b). Metal-CO_2 electrochemistry: From CO_2 recycling to energy storage. *Adv. Energy Mater.* 11 (25), 2100667. doi:10.1002/aenm.202100667

Wang, G.-D., Wang, H.-H., Shi, W.-J., Hou, L., Wang, Y.-Y., and Zhu, Z. (2021c). A highly stable MOF with F and N accessible sites for efficient capture and separation of acetylene from ternary mixtures. *J. Mater. Chem. A* 9 (43), 24495–24502. doi:10.1039/d1ta05720k

Wang, H. F., Chen, L., Pang, H., Kaskel, S., and Xu, Q. (2020a). MOF-derived electrocatalysts for oxygen reduction, oxygen evolution and hydrogen evolution reactions. *Chem. Soc. Rev.* 49 (5), 1414–1448. doi:10.1039/c9cs00906j

Wang, H., Wu, Q., Cheng, L., Chen, L., Li, M., and Zhu, G. (2022a). Porphyrin- and phthalocyanine-based systems for rechargeable batteries. *Energy Storage Mater.* 52, 495–513. doi:10.1016/j.ensm.2022.08.022

Wang, J., Kong, H., Zhang, J., Hao, Y., Shao, Z., and Ciucci, F. (2021d). Carbon-based electrocatalysts for sustainable energy applications. *Prog. Mater. Sci.* 116, 100717. doi:10.1016/j.pmatsci.2020.100717

Wang, J., Zheng, X., Wang, G., Cao, Y., Ding, W., Zhang, J., et al. (2022c). Defective bimetallic selenides for selective CO_2 electroreduction to CO. Adv. Mater *(2022b)* 34 (3), e2106354. doi:10.1002/adma.202106354

Wang, K., Wu, Y., Cao, X., Gu, L., and Hu, J. (2020b). A Zn-CO_2 flow battery generating electricity and methane. *Adv. Funct. Mater.* 30 (9), 1908965. doi:10.1002/adfm.201908965

Wang, Q., and Astruc, D. (2020). State of the art and prospects in metal-organic framework (MOF)-Based and MOF-derived nanocatalysis. *Chem. Rev.* 120 (2), 1438–1511. doi:10.1021/acs.chemrev.9b00223

Wang, R., Li, X., Nie, Z., Zhao, Y., and Wang, H. (2021e). Metal/metal oxide nanoparticles-composited porous carbon for high-performance supercapacitors. *J. Energy Storage* 38, 102479. doi:10.1016/j.est.2021.102479

Wang, T., Sang, X., Zheng, W., Yang, B., Yao, S., Lei, C., et al. (2020c). Gas diffusion strategy for inserting atomic iron sites into graphitized carbon supports for unusually high-efficient CO_2 electroreduction and high-performance Zn-CO_2 batteries. *Adv. Mater* 32 (29), e2002430. doi:10.1002/adma.202002430

Wang, X., Hu, J.-M., and Hsing, I. M. (2004). Electrochemical investigation of formic acid electro-oxidation and its crossover through a Nafion® membrane. *J. Electroanal. Chem.* 562 (1), 73–80. doi:10.1016/j.jelechem.2003.08.010

Wang, X., Xie, J., Ghausi, M. A., Lv, J., Huang, Y., Wu, M., et al. (2019). Rechargeable Zn-CO_2 electrochemical cells mimicking two-step photosynthesis. *Adv. Mater* 31 (17), e1807807. doi:10.1002/adma.201807807

Wang, Y.-X., Rinawati, M., Huang, W.-H., Cheng, Y.-S., Lin, P.-H., Chen, K.-J., et al. (2022b). Surface-engineered N-doped carbon nanotubes with B-doped graphene quantum dots: Strategies to develop highly-efficient noble metal-free electrocatalyst for online-monitoring dissolved oxygen biosensor. *Carbon* 186, 406–415. doi:10.1016/j.carbon.2021.10.027

Wang, Y., Huang, Z., Lei, Y., Wu, J., Bai, Y., Zhao, X., et al. (2022d). Bismuth with abundant defects for electrocatalytic CO_2 reduction and Zn-CO_2 batteries. *Chem. Commun. (Camb)* 58 (22), 3621–3624. doi:10.1039/d2cc00114d

Wang, Y., Liu, Y., Liu, W., Wu, J., Li, Q., Feng, Q., et al. (2020d). Regulating the coordination structure of metal single atoms for efficient electrocatalytic CO_2 reduction. *Energy and Environ. Sci.* 13 (12), 4609–4624. doi:10.1039/d0ee02833a

Wu, M., Zhang, G., Yang, H., Liu, X., Dubois, M., Gauthier, M. A., et al. (2021). Aqueous Zn-based rechargeable batteries: Recent progress and future perspectives. *InfoMat*. doi:10.1002/inf2.12265

Xiang Li, S. Y., Feng, N., He, P., and Zhou, H. (2016). Progress in research on Li-CO_2 batteries: Mechanism, catalyst and performance. *Chin. J. Catal.* 37, 1016–1024. doi:10.1016/S1872-2067(15)61125-1

Xie, J., Huang, Y., Wu, M., and Wang, Y. (2019). Electrochemical carbon dioxide splitting. *ChemElectroChem* 6 (6), 1587–1604. doi:10.1002/celc.201801716

Xie, J., Wang, X., Lv, J., Huang, Y., Wu, M., Wang, Y., et al. (2018a). Reversible aqueous zinc-CO_2 batteries based on CO_2-HCOOH interconversion. *Angew. Chem. Int. Ed. Engl.* 57 (52), 16996–17001. doi:10.1002/anie.201811853

Xie, J., and Wang, Y. (2019). Recent development of CO_2 electrochemistry from Li-CO_2 batteries to Zn-CO_2 batteries. *Acc. Chem. Res.* 52 (6), 1721–1729. doi:10.1021/acs.accounts.9b00179

Xie, J., Zhao, X., Wu, M., Li, Q., Wang, Y., and Yao, J. (2018b). Metal-free fluorine-doped carbon electrocatalyst for CO_2 reduction outcompeting hydrogen evolution. *Angew. Chem. Int. Ed. Engl.* 57 (31), 9640–9644. doi:10.1002/anie.201802055

Xiong, Y., Dong, J., Huang, Z. Q., Xin, P., Chen, W., Wang, Y., et al. (2020). Single-atom Rh/N-doped carbon electrocatalyst for formic acid oxidation. *Nat. Nanotechnol.* 15 (5), 390–397. doi:10.1038/s41565-020-0665-x

Xu, H., Cheng, D., Cao, D., and Zeng, X. C. (2018). A universal principle for a rational design of single-atom electrocatalysts. *Nat. Catal.* 1 (5), 339–348. doi:10.1038/s41929-018-0063-z

Xue Teng, Y. N., Gong, S., Xuan, L., and Chen, Z. (2021). Selective CO_2 reduction to formate on heterostructured Sn/SnO_2 nanoparticles promoted by carbon layer networks. *J. Electrochem.* 2022, 27. doi:10.13208/j.electrochem.210844

Xue, X., Yang, H., Yang, T., Yuan, P., Li, Q., Mu, S., et al. (2019). P-coordinated fullerene-like carbon nanostructures with dual active centers toward highly-efficient multi-functional electrocatalysis for CO_2RR, ORR and Zn-air battery. *J. Mater. Chem. A* 7 (25), 15271–15277. doi:10.1039/c9ta03828k

Yan, C., Li, H., Ye, Y., Wu, H., Cai, F., Si, R., et al. (2018). Coordinatively unsaturated nickel-nitrogen sites towards selective and high-rate CO_2 electroreduction. *Energy and Environ. Sci.* 11 (5), 1204–1210. doi:10.1039/c8ee00133b

Yan, S., Peng, C., Yang, C., Chen, Y., Zhang, J., Guan, A., et al. (2021). Electron localization and lattice strain induced by surface lithium doping enable ampere-level electrosynthesis of formate from CO_2. *Angew. Chem. Int. Ed. Engl.* 60 (49), 25741–25745. doi:10.1002/anie.202111351

Yang, D., Chen, D., Jiang, Y., Ang, E. H., Feng, Y., Rui, X., et al. (2020a). Carbon-based materials for all-solid-state zinc-air batteries. *Carbon Energy* 3 (1), 50–65. doi:10.1002/cey2.88

Yang, D., Zhu, Q., Chen, C., Liu, H., Liu, Z., Zhao, Z., et al. (2019a). Selective electroreduction of carbon dioxide to methanol on copper selenide nanocatalysts. *Nat. Commun.* 10 (1), 677. doi:10.1038/s41467-019-08653-9

Yang, H. B., Hung, S.-F., Liu, S., Yuan, K., Miao, S., Zhang, L., et al. (2018). Atomically dispersed Ni (I) as the active site for electrochemical CO_2 reduction. *Nat. Energy* 3 (2), 140–147. doi:10.1038/s41560-017-0078-8

Yang, H., Chang, Z., Qiao, Y., Deng, H., Mu, X., He, P., et al. (2020b). Constructing a super-saturated electrolyte front surface for stable rechargeable aqueous zinc batteries. *Angew. Chem. Int. Ed. Engl.* 59 (24), 9377–9381. doi:10.1002/anie.202001844

Yang, J., Guo, D., Zhao, S., Lin, Y., Yang, R., Xu, D., et al. (2019b). Cobalt phosphides nanocrystals encapsulated by P-doped carbon and married with P-doped graphene for overall water splitting. *Small* 15 (10), e1804546. doi:10.1002/smll.201804546

Yang, M., Liu, S., Sun, J., Jin, M., Fu, R., Zhang, S., et al. (2022a). Highly dispersed Bi clusters for efficient rechargeable Zn-CO_2 batteries. *Appl. Catal. B Environ.* 307, 121145. doi:10.1016/j.apcatb.2022.121145

Yang, R., Xie, J., Liu, Q., Huang, Y., Lv, J., Ghausi, M. A., et al. (2019c). A trifunctional Ni-N/P-O-codoped graphene electrocatalyst enables dual-model rechargeable Zn-CO_2/Zn-O_2 batteries. *J. Mater. Chem. A* 7 (6), 2575–2580. doi:10.1039/c8ta10958c

Yang, X., Zhang, C., Chai, L., Zhang, W., and Li, Z. (2022b). Bimetallic rechargeable Al/Zn hybrid aqueous batteries based on Al-Zn alloys with composite electrolytes. *Adv. Mater* 34 (45), e2206099. doi:10.1002/adma.202206099

Ye, K., Zhou, Z., Shao, J., Lin, L., Gao, D., Ta, N., et al. (2020). *In situ* reconstruction of a hierarchical Sn-Cu/SnOx core/shell catalyst for high-performance CO_2 electroreduction. *Angew. Chem. Int. Ed. Engl.* 59 (12), 4814–4821. doi:10.1002/anie.201916538

Yu, J., Feng, H., Tang, L., Pang, Y., Zeng, G., Lu, Y., et al. (2020). Metal-free carbon materials for persulfate-based advanced oxidation process: Microstructure, property and tailoring. *Prog. Mater. Sci.* 111, 100654. doi:10.1016/j.pmatsci.2020.100654

Yuan, Y., and Lu, J. (2019). Demanding energy from carbon. *Carbon Energy* 1 (1), 8–12. doi:10.1002/cey2.12

Yujie Shi, Y. Z., and Lou, Y. (2022). * zupeng chen, haifeng Xiong, and yongfa Zhu*. Homogeneity of supported single-atom active sites boosting the selective catalytic transformations. *Adv. Sci. (Weinh)* 55, 40. doi:10.1002/advs.202201520

Zeng, Z., Mohamed, A. G. A., Zhang, X., and Wang, Y. (2021). Wide potential CO_2-to-CO electroreduction relies on pyridinic-N/Ni-nx sites and its Zn-CO_2 battery application. *Energy Technol.* 9 (8), 2100205. doi:10.1002/ente.202100205

Zhang, L., Han, L., Liu, H., Liu, X., and Luo, J. (2017). Back cover: Potential-cycling synthesis of single platinum atoms for efficient hydrogen evolution in neutral media (angew. Chem. Int. Ed. 44/2017) *Angew. Chem. Int. Ed.* 56 (44), 13900. doi:10.1002/anie.201709950

Zhang, N., Zhang, X., Tao, L., Jiang, P., Ye, C., Lin, R., et al. (2021a). Silver single-atom catalyst for efficient electrochemical CO_2 reduction synthesized from thermal transformation and surface reconstruction. *Angew. Chem. Int. Ed. Engl.* 60 (11), 6170–6176. doi:10.1002/anie.202014718

Zhang, S., Wang, J., Wang, J., Wang, K. Y., Zhao, M., Zhang, L., et al. (2022). A gradient Sn^{4+}@Sn^{2+} core@shell structure induced by a strong metal oxide-support interaction for enhanced CO_2 electroreduction. *Dalton Trans.* 51 (42), 16135–16144. doi:10.1039/d2dt02788g

Zhang, Y., Jiao, L., Yang, W., Xie, C., and Jiang, H. L. (2021b). Rational fabrication of low-coordinate single-atom Ni electrocatalysts by MOFs for highly selective CO_2 reduction. *Angew. Chem. Int. Ed. Engl.* 60 (14), 7607–7611. doi:10.1002/anie.202016219

Zhao, D., Zhu, Y., Wu, Q., Zhou, W., Dan, J., Zhu, H., et al. (2022a). Low-loading Ir decorated cobalt encapsulated N-doped carbon nanotubes/porous carbon sheet implements efficient hydrogen/oxygen trifunctional electrocatalysis. *Chem. Eng. J.* 430, 132825. doi:10.1016/j.cej.2021.132825

Zhao, M., Feng, J., Yang, W., Song, S., and Zhang, H. (2020). Recent advances in graphitic carbon nitride supported single-atom catalysts for energy conversion. *ChemCatChem* 13 (5), 1250–1270. doi:10.1002/cctc.202001517

Zhao, S. N., Li, J. K., Wang, R., Cai, J., and Zang, S. Q. (2022b). Electronically and geometrically modified single-atom Fe sites by adjacent Fe nanoparticles for enhanced oxygen reduction. *Adv. Mater* 34 (5), e2107291. doi:10.1002/adma.202107291

Zheng, W., Yang, J., Chen, H., Hou, Y., Wang, Q., Gu, M., et al. (2019). Atomically defined undercoordinated active sites for highly efficient CO_2 electroreduction. *Adv. Funct. Mater.* 30 (4), 1907658. doi:10.1002/adfm.201907658

Zhong, C., Liu, B., Ding, J., Liu, X., Zhong, Y., Li, Y., et al. (2020). Decoupling electrolytes towards stable and high-energy rechargeable aqueous zinc–manganese dioxide batteries. *Nat. Energy* 5 (6), 440–449. doi:10.1038/s41560-020-0584-y

Zhou, J., Cheng, J., Wang, B., Peng, H., and Lu, J. (2020). Flexible metal-gas batteries: A potential option for next-generation power accessories for wearable electronics. *Energy and Environ. Sci.* 13 (7), 1933–1970. doi:10.1039/d0ee00039f

Zhou, Y., Chen, G., Wang, Q., Wang, D., Tao, X., Zhang, T., et al. (2021). Fe-N-C electrocatalysts with densely accessible Fe-N_4 sites for efficient oxygen reduction reaction. *Adv. Funct. Mater.* 31 (34), 2102420. doi:10.1002/adfm.202102420

Zhou, Z.-Y., and Sun, S.-G. (2017). A breakthrough in electrocatalysis of CO_2 conversion. *Natl. Sci. Rev.* 4 (2), 155–156. doi:10.1093/nsr/nww083

Zhu, Y., Pan, Y., Zhu, Y., Jiang, H., Shen, J., and Li, C. (2021a). Efficient electrocatalytic formic acid oxidation over PdAu-manganese oxide/carbon. *J. Colloid Interface Sci.* 593, 244–250. doi:10.1016/j.jcis.2021.02.110

Zhu, Y., Yuk, S. F., Zheng, J., Nguyen, M. T., Lee, M. S., Szanyi, J., et al. (2021b). Environment of metal-O-Fe bonds enabling high activity in CO_2 reduction on single metal atoms and on supported nanoparticles. *J. Am. Chem. Soc.* 143 (14), 5540–5549. doi:10.1021/jacs.1c02276

Zhuang, Z., Kang, Q., Wang, D., and Li, Y. (2020). Single-atom catalysis enables long-life, high-energy lithium-sulfur batteries. *Nano Res.* 13 (7), 1856–1866. doi:10.1007/s12274-020-2827-4